

TECHNICAL NOTE D-2070) OTS: \$ 1.50
(NASA TN)

A NUMERICAL ANALYSIS OF DIRECT NUCLEAR ELECTROGENERATOR
CELLS THAT USE CERIUM 144 BETA-EMITTING
RADIOISOTOPE SOURCES

By Allan J. Cohen *Washington, NASA, Nov. 1963 58p refs*

NASA

Lewis Research Center
Cleveland, Ohio

NATIONAL AERONAUTICS AND SPACE ADMINISTRATION

A NUMERICAL ANALYSIS OF DIRECT NUCLEAR ELECTROGENERATOR
CELLS THAT USE CERIUM 144 BETA-EMITTING

RADIOISOTOPE SOURCES

By Allan J. Cohen

SUMMARY

2368.3

An analysis of a radioisotope electric cell that uses the beta emitter, cerium 144, was undertaken. The analysis, which relies on formats set forth for fission electric cells, takes into account the pertinent physical constraints in a more accurate manner than has been done previously. Results from the analysis are presented in tables and as representative plots. Comparisons between accurate and approximate solutions are also included.

~~2368.3~~
NUT/1012

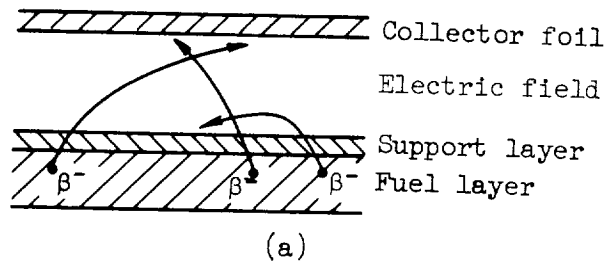
INTRODUCTION

Presently there exists a growing interest in the production of large quantities of electric power at low specific weights for use in electric propulsion systems. Recently an electric powerplant design in the form of a battery that converts the energy of decaying radioisotopes directly into electric power has been proposed (ref. 1). The most desirable feature of such a cell is its low-weight to power-output ratio (lb/kw). A further characteristic of the cell is its requirement of a colloidal-particle thruster because of the high voltage generated. This thruster, although presently in an early research stage, shows high theoretical efficiencies over a large range of specific impulse (ref. 2).

In the original paper (ref. 1) on space radioisotope cell designs, calculations were performed from information available on fission electric cells (refs. 3 and 4). This previous study included calculations of operating voltage, cell efficiency, weight per unit power output, and component temperature. Since the basic analysis on fission electric cells yielded a limited amount of pertinent information, the study was approximate and incomplete, and consequently a more exact analysis of the cell was undertaken. This analysis is concerned with a steady-state operation of radioisotope cells that use the beta-emitting radioisotope, cerium 144. A discussion relevant to the choice of this beta-emitting radioisotope appears in reference 5. The present report describes in detail the analytical method and presents the basic results of the computations performed numerically on the IBM 7090 at the Lewis Research Center. Portions of these results were previously summarized in reference 6.

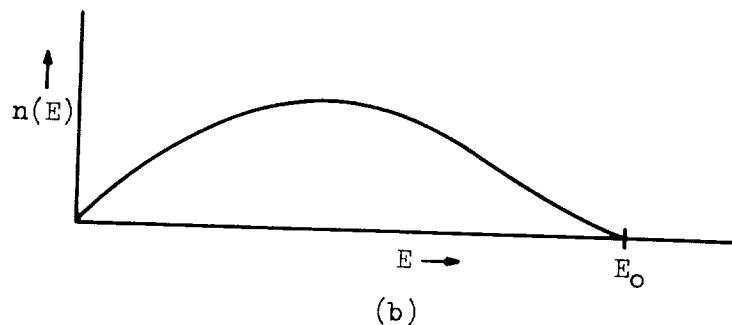
ANALYSIS

The operating principles of the radioisotope electrogenerator are as follows: Beta particles (electrons), as depicted in sketch (a), are emitted in all



directions from the radioisotope fuel layer. The energetic beta particles travel through the fuel layer and out through a covering support layer. At this point beta particles with sufficient energy travel across the vacuum gap to the collector foil. In this action the emitter becomes positively charged and the collector becomes negatively charged, thus producing a potential field across the cell. It is in the crossing of this potential field that the kinetic energy of the beta particle is converted directly into electrical energy. In steady-state operation, the flow of current from the collector is compensated for by the internal flow of beta particles to the collector. Further descriptions of the proposed operation of the radioisotope electrogenerator in an electrostatic propulsion system are given in references 1, 5, and 6.

Operation of the cell depends on the emission of highly energetic beta particles by the radioisotope. In this radioactive decay process, beta particles are emitted over a continuous spectrum of energy. Sketch (b) shows a typical beta spectrum with $n(E)$ representing the number of emitted beta particles per unit energy and E the energy of these beta particles. (All symbols are defined in the appendix.) An outstanding feature of the beta spectrum is that it has a



maximum energy called the end-point energy (denoted as E_0). Each beta-emission process is characterized by a unique end-point energy. A theoretical analysis of the beta-emission process yields the relation (ref. 7):

$$\left. \begin{aligned} n(\epsilon) &\approx \epsilon \sqrt{\epsilon^2 - 1} (\epsilon_0 - \epsilon)^2 \\ \epsilon &\equiv \frac{m_0 c^2 + E}{E} \end{aligned} \right\} \quad (1)$$

where

$m_0 c^2$ rest energy of electron

E energy, Mev

ϵ_0 value of ϵ for $E = E_0$

which holds for an allowed nuclear transition. This report considers only the 2.98-Mev beta particle emitted from the radioisotope chain, cerium - praseodymium 144. It has been experimentally shown (ref. 8) that this beta emission can be represented by a Kurie plot and thus should follow the relation (eq. (1)) for an allowed nuclear transition.

Since the rest energy of the beta particle is 0.511 Mev, well within the limits of the beta decaying energies considered in the analysis, the relativistic correction must be considered. Therefore, to attain an accurate description of the cell parameters, the relativistic formulations of the equations of motion for particles are used throughout this report.

In addition to these physical limits, the problem of high-energy electrons traveling through materials must be considered. It will be assumed that the energetic electrons travel in a straight path (negligible scattering) and that they lose a fixed energy for a given travel distance (negligible straggling). In the present problem, these assumptions do not appear to be critical, since it can be argued that electron scattering and straggling will average out in the intended integrations.

The Katz-Penfold relation (ref. 9)

$$R_p = 412 E^{1.265 - 0.0954 \ln E} \quad \text{mg/cm}^2 \quad (2)$$

predicts the practical range R_p (effective straight-line distance in which an electron loses its entire initial energy) for an electron of a fixed initial energy E (below 3 Mev). This is the best range-energy relation available for electrons and is a result of experiments (ref. 9) of electron energy loss in aluminum. By multiplying by the factor $\left(\frac{A}{Z} \frac{13}{27}\right)$ (ref. 10) the Katz-Penfold relation becomes applicable to elements other than aluminum. This form of the relation is used in the present report to predict electron energy loss in the support and fuel layers of the radioisotope cell.

It has been observed as a result of the present investigation that the use of nonrelativistic equations in place of their relativistic counterparts and the

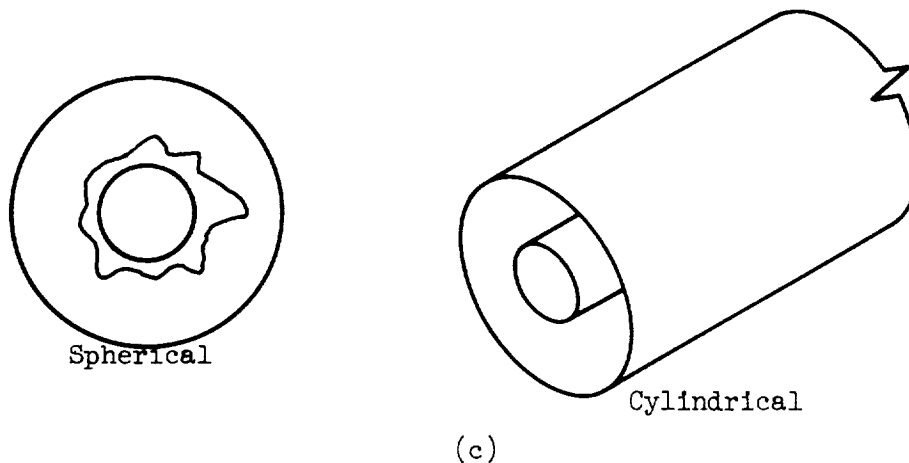
use of a linear approximation to the Katz-Penfold relation yielded results that compared closely with the nonapproximated results (see comparative section Effects of Changes in Physical Relations). In view of this fact, the analysis that follows includes these approximate forms of the physical constraints.

In the analysis of the direct nuclear electrogenerator cell, the following quantities are of interest:

n	number of beta particles reaching collector per second per unit emitter area
η	electric efficiency of cell
E_c	total energy of beta particles reaching collector per second per unit emitter area
$D(\gamma, E_{p,c})$	distribution of beta particles reaching collector per second per unit emitter area as a function of their arrival angle and energy

These parameters are important to the design of the electrogenerator cell. From plots of n against cell voltage, an operating point can be deduced. The procedure for deriving this operating voltage is outlined in the section Number of Particles Reaching Collector. The importance of the electric efficiency is that it yields the value of the weight per unit power output for a particular cell - a measure of the applicability of the cell to space electric propulsion. Since the cell has three major parts (discussed subsequently), the emitter, the collector, and the vacuum gap, a knowledge of η and E_c is all that is necessary in obtaining the entire distribution of energy in an operating cell. Finally, the quantity $D(\gamma, E_{p,c})$ is important in considering the magnitude of backscattered electrons at the collector surface of the cell.

Two cell geometries (see sketch (c)), the spherical concentric and the coaxial cylindrical, are considered. The cells consist of two foils - an emitter



foil as the inside element and a collector foil as the outside surface. The emitter foil contains a fuel layer of the beta-emitting radioisotope, cerium 144, spread uniformly over the inside of a support foil. The collector is simply a single foil that encloses the electric field.

For the purpose of the analysis, the following additional assumptions are made:

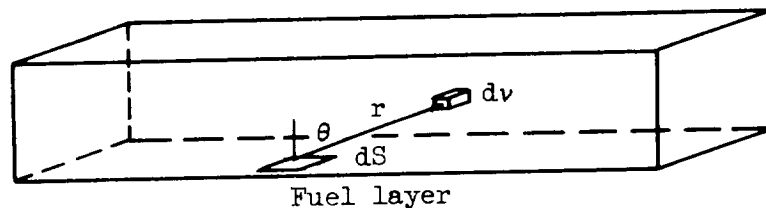
- (1) The curvature of the fuel layer is disregarded (very thin fuel layers, relative to the radii, will be considered).
- (2) The cell is operating at steady state.
- (3) End effects in the cylindrical configuration are not considered.
- (4) Secondary electron and backscattering effects are neglected.
- (5) Additional design structures (insulators, separators, connectors, etc.) are neglected.

All these conditions, it is hoped, can be approached in the actual cell design.

SPHERICAL CONFIGURATION

Number of Particles Reaching Collector

A section of the fuel layer is depicted in sketch (d). Beta particles are



(d)

emitted from an arbitrary volume element dv , and a portion of them will leave the fuel layer through a unit segment of the surface dS . Since the charged beta particles are emitted uniformly in all spatial directions, the total number dn'_e per second passing through dS and reaching the collector is

$$\left. \begin{aligned} dn'_e &= \frac{dS \cos \theta}{4\pi r^2} N_e dv & \text{for } r \leq r_{\max} \\ dn'_e &= 0 & \text{for } r > r_{\max} \end{aligned} \right\} \quad (3)$$

where N_e is the number of emitted beta particles per second per unit volume

with an energy E_β , and r_{\max} (a function of the angle θ) is some calculated distance to be evaluated later.

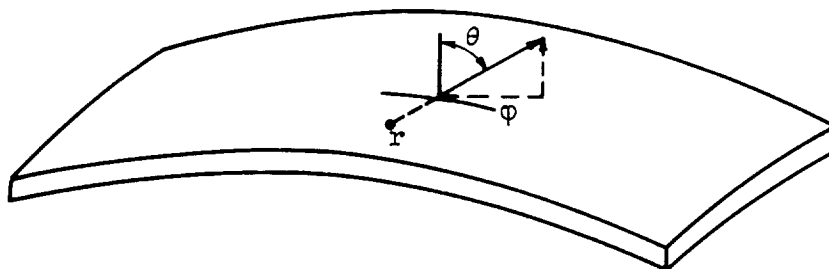
The element of volume in spherical coordinates is

$$dV = r^2 \sin \theta \, dr \, d\theta \, d\phi \quad (4)$$

and thus equation (3) expands to

$$dn'_\epsilon = \frac{N_\epsilon}{4\pi} \cos \theta \sin \theta \, dS \, dr \, d\theta \, d\phi \quad (5)$$

For the spherical configuration, the coordinate system is best oriented as shown in sketch (e).



(e)

Hence, the number of particles per second leaving the fuel layer per unit area and reaching the collector is

$$n_\epsilon = \frac{N_\epsilon}{4\pi} \int_0^{2\pi} d\phi \int_0^{\theta_{\max}} d\theta \int_0^{r_{\max}(\theta)} dr \sin \theta \cos \theta \quad (6)$$

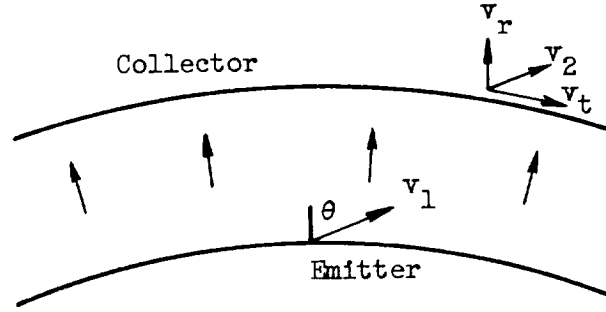
where the limits r_{\max} and θ_{\max} are the values of r and θ beyond which there are no further contributions to the integral. (The meaning and the evaluation of the limits will be discussed more fully in the following paragraphs.) Moreover, since the geometry being considered has spherical symmetry, equation (6) reduces to

$$n_\epsilon = \frac{N_\epsilon}{2} \int_0^{\theta_{\max}} d\theta \int_0^{r_{\max}(\theta)} dr \sin \theta \cos \theta \quad (7)$$

Since the beta particles lose energy in crossing the electric field of the cell and also lose energy in traveling through the emitter foil, not all the beta

particles have sufficient initial energy to reach the collector. With this in mind, it can be seen that the limits of integration, $r_{\max}(\theta)$ and θ_{\max} , are the values of r and θ beyond which the initial energy of the beta particles is insufficient to carry them to the collector.

The problem of finding $r_{\max}(\theta)$ and θ_{\max} may now be considered. Sketch (f) represents the electric field through which beta particles travel from emitter to collector.



(f)

On introducing the following definitions,

- U kinetic energy of beta particle
- Φ cell voltage
- e electronic charge
- P_t linear momentum, tangential direction
- R_1, R_2 inner and outer radii, respectively

the equations of motion for the beta particle in the radial electric field of the cell can be written as

$$U_1 = U_2 + e\Phi \quad (\text{conservation of energy}) \quad (8)$$

$$R_1 P_{t,1} = R_2 P_{t,2} \quad (\text{conservation of angular momentum}) \quad (9)$$

where the subscripts 1 and 2 refer to the initial (emitter) and final (collector) values.

To find the minimum initial kinetic energy $U_{1,\min}$ for which the beta particle can still reach the collector, the radial velocity at the collector $v_{r,2}$ is set equal to zero. With this stipulation ($v_{r,2} = 0$) the relativistic form of equations (8) and (9) is:

$$m_0 c^2 \left[\frac{1}{\sqrt{1 - \left(\frac{v_{l,min}}{c}\right)^2}} - 1 \right] = m_0 c^2 \left[\frac{1}{\sqrt{1 - \left(\frac{v_t}{c}\right)^2}} - 1 \right] + e\Phi \quad (10a)$$

$$\frac{m_0 v_{l,min} \sin \theta}{\sqrt{1 - \left(\frac{v_{l,min}}{c}\right)^2}} R_1 = \frac{m_0 v_t}{\sqrt{1 - \left(\frac{v_t}{c}\right)^2}} R_2 \quad (11a)$$

where $v_{l,min}$ is the minimum initial velocity of the beta particle and m_0 its mass. Eliminating v_t (tangential velocity at the collector) yields

$$(U_{l,min} + U_0 - e\Phi)^2 - U_0^2 = \left[(U_{l,min} + U_0)^2 - U_0^2 \right] \left(\frac{R_1}{R_2} \right)^2 \sin^2 \theta \quad (12a)$$

where $U_0 = m_0 c^2$ is the rest mass energy and $U_{l,min} = U_0 \left[\frac{1}{\sqrt{1 - \frac{v_{l,min}^2}{c^2}}} - 1 \right]$

is the minimum initial kinetic energy that a particle must have to cross the electric field for a given angle θ .

In the nonrelativistic formulation of the problem, equations (10a) and (11a) have the following counterparts:

$$\left(\frac{1}{2} m_0 v_{l,min}^2 \right) = \frac{1}{2} m_0 v_t^2 + e\Phi \quad (10b)$$

$$m_0 R_1 v_{l,min} \sin \theta = m_0 R_2 v_t \quad (11b)$$

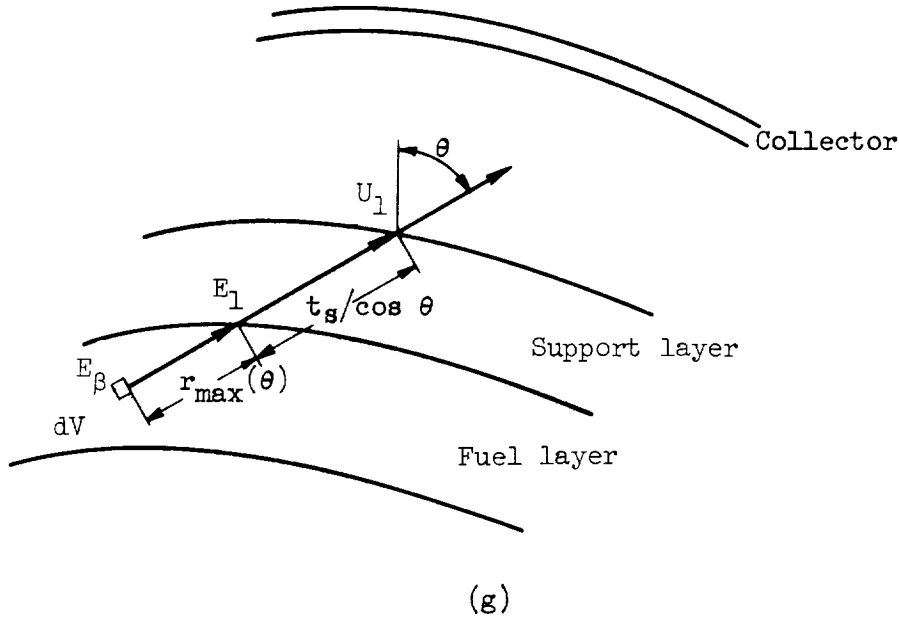
which, on eliminating v_t between them, reduce to

$$\left(\frac{1}{2} m_0 v_{l,min}^2 \right) \left[1 - \left(\frac{R_1}{R_2} \right)^2 \sin^2 \theta \right] = e\Phi \quad (12b)$$

Equation (12b) corresponds to equation (12a) with $\left(\frac{1}{2} m_0 v_{l,min}^2 \right)$ equivalent to the quantity $U_{l,min}$ and is more readily solvable than equation (12a) for the desired minimum beta-particle energy term.

Now to complete the problem of obtaining the limits of integration, $r_{max}(\theta)$ and θ_{max} , it is necessary only to consider the effect of energy loss in the

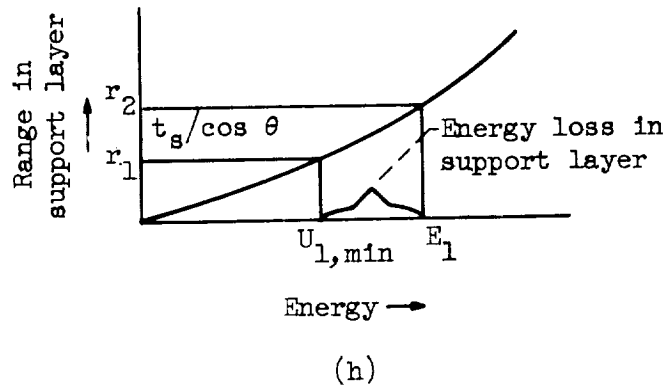
emitter foil (support and fuel layer). Sketch (g) shows the path of the beta particle through the emitter foils with values of energy placed at the base of



each vector. Since the beta particle loses energy in passing a distance $t_s / \cos \theta$ through the support layer, its entrance energy E_1 must be larger than $U_{1,min}$ by just the amount of this loss. Expressing the range-energy relation as $R = f(E)$ means the condition (see sketch (h))

$$\frac{t_s}{\cos \theta} = f(E_1) - f(U_{1,min}) \quad (13)$$

must be satisfied and can be evaluated to obtain the quantity E_1 . If the beta particle having the energy E_β at birth needs only the energy E_1 (to reach

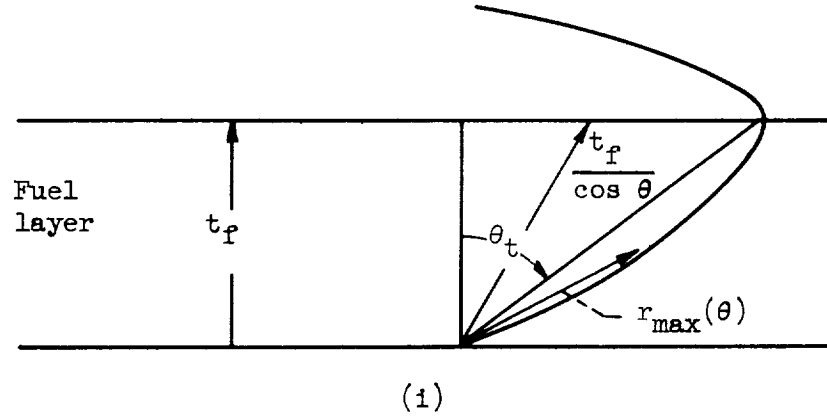


the collector) on entering the support layer, its maximum travel distance in the fuel layer $r_{\max}(\theta)$ is

$$r_{\max}(\theta) = f(E_\beta) - f(E_1) \quad (14)$$

The limit θ_{\max} is simply the angle for which $r_{\max}(\theta)$ first becomes zero. This procedure, including the evaluation of $U_{1,\min}(\theta)$, may be carried out separately for each angle θ .

The limits of integration $r_{\max}(\theta)$ and θ_{\max} derived in the preceding manner must be modified by the geometry of the fuel layer. The integration over the coordinate r must not exceed the boundary of the fuel layer (see sketch (i)).



Thus, $r_{\max}(\theta)$ is taken as the smaller of $t_f / \cos \theta$ or $r_{\max}(\theta)$ (calculated) where t_f is the fuel-layer thickness. Because of this duality, a cutoff angle θ_t exists that satisfies the relation

$$\left. \begin{aligned} \cos \theta_t &= \frac{t_f}{r_{\max}(\theta_t)} & \text{for } \theta_t > 0 \\ 1 &\leq \frac{t_f}{r_{\max}(0)} & \text{for } \theta_t = 0 \end{aligned} \right\} \quad (16)$$

The maximum value of θ must not exceed $\pi/2$; thus, θ_{\max} is taken as the smaller of $\pi/2$ or θ_{\max} (calculated). Now the integral for n_e takes the form

$$n_e = \frac{N_e}{2} \left(\int_{\theta_t}^{\theta_{\max}} d\theta \int_0^{r_{\max}(\theta)} \sin \theta \cos \theta dr + \int_0^{\theta_t} d\theta \int_0^{t_f / \cos \theta} \sin \theta \cos \theta dr \right) \quad (17)$$

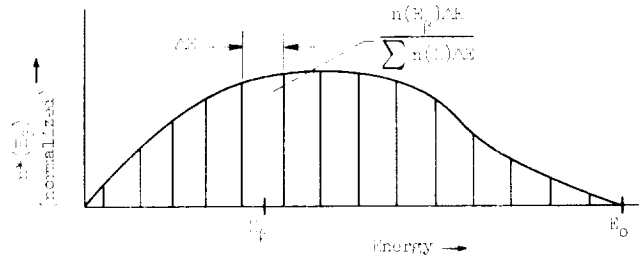
which reduces to

$$n_e = \frac{N_e}{2} \left[\int_{\theta_t}^{\theta_{\max}} r_{\max}(\theta) \sin \theta \cos \theta + t_f(1 - \cos \theta_t) d\theta \right] \quad (18)$$

where θ_{\max} must not exceed $\pi/2$.

Modifications to Parameter Analysis

It is appropriate at this point to consider the effects of the beta spectrum on the parameter calculations. As discussed previously, beta particles are emitted over a range or spectrum of energies. The spectrum is continuous, ranging from zero energy to a maximum or end-point energy. From the end-point energy an expression (eq. (1)) can be derived for a weight factor $n(E_\beta)$, which, when plotted, graphically represents the beta spectrum. The beta spectrum can be divided into parts, each of which, as depicted in sketch (j), represents the percentage of beta particles emitted in an energy segment and each of which is represented by its midpoint energy E_β . Thus, in calculating n , the number of



(j)

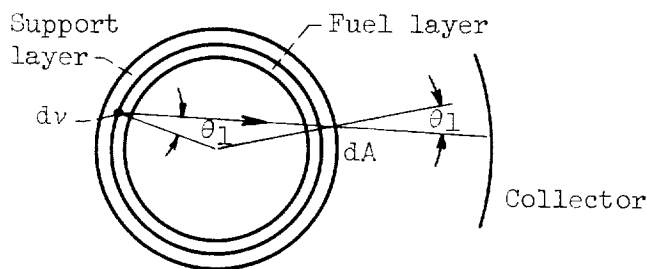
particles reaching the collector, the calculation proceeds for each E_β with

$$N_e \rightarrow Nn^*(E_\beta)$$

(where $*$ refers to the normalized quantity) and then these partial results are summed over the appropriate normalizing factor. Hence, n takes the form

$$n = \frac{N \sum_{E_\beta} \frac{n(E_\beta)}{2} \left[\int_{\theta_t}^{\theta_{\max}} r_{\max} \sin \theta \cos \theta + t_f(1 - \cos \theta_t) d\theta \right] \Delta E}{\sum_{E_\beta} n(E_\beta) \Delta E} \quad (19)$$

In addition to the spectrum effect on the calculation, there exists another effect that must be considered at this point. As can be seen in sketch (k), beta particles emitted in the "backward" direction can reach the collector by



(k)

passing through the opposite side of the emitter (assuming no backscattering). This effect can be handled in a rather simple way. These particles increase the number of particles in the forward direction by an amount just equal to an increase that would be caused by doubling the fuel thickness. Thus, in the calculations

$$t_f \text{ (calculations)} = 2 \text{ times actual fuel-layer thickness} \quad (20)$$

which will be used in all particle computations. The proof of this assertion rests on the fact that the two angles θ_1 made with the surface of the emitter by a particle described are equal for spherical and cylindrical configurations.

Total Energy Reaching Collector

If dn_ϵ is the number of particles per second per unit emitter area reaching the collector from a volume element dv with an energy $E_{p,c}$, the total energy per second per unit emitter area reaching the collector is

$$(E_c)_\epsilon = \int_{\text{volume}} E_{p,c} dn_\epsilon \quad (21)$$

which becomes, after substituting for dn_ϵ and summing over the energy spectrum,

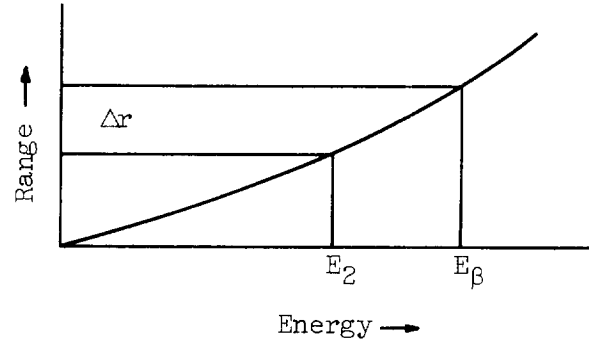
$$E_c = \left\{ \sum_{\beta} n(E_\beta) \left[\int_{\theta_t}^{\theta_{\max}} d\theta \int_0^{r_{\max}(\theta)} E_{p,c}(r,\theta) \sin \theta \cos \theta dr \right. \right. \\ \left. \left. + \int_0^{\theta_t} d\theta \int_0^{t_f \sec \theta} E_{p,c}(r,\theta) \sin \theta \cos \theta dr \right] \Delta E \right\} / \sum n(E_\beta) \Delta E \quad (22)$$

The energy $E_{p,c}(r,\theta)$ is determined from

$$E_{p,c} = E_{\beta} - (E_f + E_s + e\Phi) \quad (23)$$

where E_f and E_s are the energies lost in the fuel and support layers, respectively.

The quantities E_f and E_s are found as follows (illustrated graphically): Sketch (l) represents a plot of range against energy for a beta particle in the

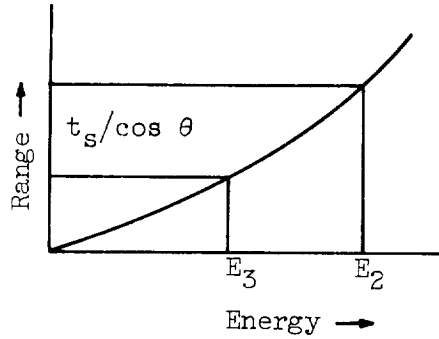


(l)

fuel layer. For a travel distance of Δr in the fuel layer (from birth to arrival at the support layer), the beta particle will lose the energy

$$E_f = E_{\beta} - E_2 \quad (24)$$

On traveling through the support layer (see range energy curve in sketch (m)),



(m)

the beta particle will lose the energy

$$E_s = E_2 - E_3 \quad (25)$$

Hence, on substituting in equations (24) and (25), equation (23) reduces to

$$E_{p,c}(r,\theta) = E_3 - e\Phi \quad (26)$$

where E_3 results from the preceding graphical calculations, and $e\Phi$ is the energy the beta particles lose in the electric field. (This process can be repeated until a set $E_{p,c}(r_1, \theta_1)$ is generated.)

Distribution of Particles at Collector

From the integral expression for n_e (eq. (7)) the following equation for Δn_e can be written as

$$\Delta n_e = \frac{N_e}{2} \sin \theta \cos \theta \Delta \theta \Delta r \quad (27)$$

This equation represents the increment of particles leaving the emitter in a ringed segment of angle $\Delta \theta$ and from a segment of fuel-layer thickness Δr . With the proper summation over the beta spectrum, equation (27) represents the distribution $D(\theta, r)$ of particles leaving the emitter. Further, staying within the limits previously set forth (eq. 17)), equation (27) represents the distribution of just those particles that reach the collector.

To obtain the desired distribution, it is necessary to convert the distribution (eq. (27)) with its dependence on r and θ to one with a dependence on $E_{p,c}$, the energy of a particle at the collector, and γ , the angle that the incoming particle at the collector has with the normal. From the previous section it can be seen that for a given Δr_1 there exists a unique $(E_{p,c})_1$. Hence for a

$$\Delta E_{p,c} = (E_{p,c})_1 - (E_{p,c})_{1+1} \quad (28)$$

there exists a

$$\Delta r = \Delta r_1 - \Delta r_{1+1} \quad (29)$$

Thus, by substituting $\Delta E_{p,c}$ for the corresponding Δr into equation (27), the distribution $D(\theta, r)$ becomes $D(\theta, E_{p,c})$, where $E_{p,c}$ is taken as the midpoint $\Delta E_{p,c}$.

From the equations of motion (eqs. (8) and (9)) set forth previously, an expression can be derived for

$$\gamma \equiv \tan^{-1} \frac{v_t}{v_r} \quad (30)$$

where v_t and v_r have previously been defined (sketch (f)). The expression

derived directly from equations (10a) and (11a) (or (10b) and (11b)) with v_r not set equal to zero is

$$\frac{1}{\sin^2 \gamma} = \left(\frac{R_2}{R_1} \right)^2 \frac{1}{\sin^2 \theta} \left[\frac{(U_1 + U_0 - \phi e)^2 - U_0^2}{(U_1 + U_0)^2 - U_0^2} \right] \quad (31a)$$

or, nonrelativistically,

$$\frac{1}{\sin^2 \gamma} = \left(\frac{R_2}{R_1} \right)^2 \frac{1}{\sin^2 \theta} \left(\frac{\frac{1}{2} m_0 v_0 - e\phi}{\frac{1}{2} m_0 v_0^2} \right) \quad (31b)$$

where U_1 (or $\frac{1}{2} m_0 v_0^2$) can be determined from

$$U_1 \text{ (or } \frac{1}{2} m_0 v_0^2) = E_{p,c} + e\phi \quad (32)$$

For a given pair, θ (midpoint of $\Delta\theta$) and $E_{p,c}$, there exists from equation (31) a γ . Hence, the distribution $D(\theta, E_{p,c})$ can be converted to $D(\gamma, E_{p,c})$, where γ is taken as the midpoint of $\Delta\gamma$, by noting that

$$\Delta\theta = \theta_1 - \theta_{1+1}$$

and

$$\Delta\gamma = \gamma_1 - \gamma_{1+1}$$

Thus, in the preceding manner, the distribution of particles against angle and energy at the collector may be obtained.

CYLINDRICAL CONFIGURATION

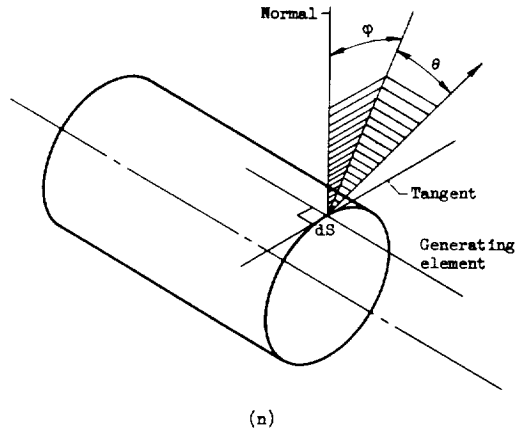
Number of Particles Reaching Collector

A spherical coordinate system for the cylindrical configuration is best set up as shown in sketch (n) (note that θ is the complement of the usual θ). The volume element becomes

$$dv = r^2 \cos \theta \, dr \, d\theta \, d\phi$$

and the projected area becomes

$$dS_p = dS \cos \theta \cos \phi$$



Thus, following the argument set forth for the spherical geometry, the expression for dn'_ϵ can be written as

$$dn'_\epsilon = \frac{N_\epsilon}{4\pi} \cos \theta \cos \phi \, dS \, dr \, d\theta \, d\phi \quad (33)$$

Continuing along, the integral for n_ϵ is

$$n_\epsilon = \frac{N_\epsilon}{\pi} \int_0^{\phi_{\max}} d\phi \int_0^{\theta_{\max}} d\theta \int_0^{r_{\max}} \cos \theta \cos \phi \, dr \quad (34)$$

where n_ϵ is the number of particles reaching the collector per second per unit emitter area, and the limits are confined to one quadrant. These limits of integration remain to be determined.

For a beta particle in the electric field of the cylindrical cell, the equations of motion can be written as (see sketch (o))

$$U_1 = U_2 + e\Phi \quad (\text{Conservation of energy}) \quad (35)$$

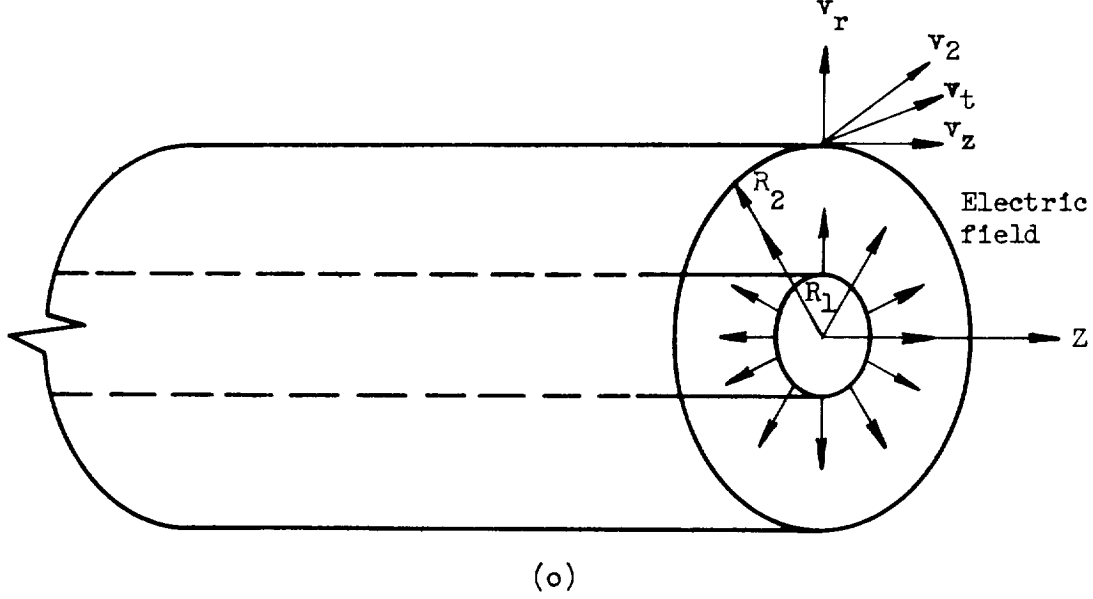
$$R_1 P_{t,1} = R_2 P_{t,2} \quad (\text{Conservation of angular momentum}) \quad (36)$$

$$P_{z,1} = P_{z,2} \quad (\text{Conservation of momentum}) \quad (37)$$

where the quantities in the equations (35) and (36) have been defined previously, and the quantity P_z is the linear momentum in the z-direction. On substituting into the equations (35) to (37) they become

$$m_0 c^2 \left[\frac{1}{\sqrt{1 - \left(\frac{v_{1,min}}{c}\right)^2}} - 1 \right] = m_0 c^2 \left(\frac{1}{\sqrt{1 - \frac{v_t^2 + v_z^2}{c^2}}} - 1 \right) + e\Phi \quad (38a)$$

$$\frac{m_o v_{l,min} \cos \theta \sin \varphi}{\sqrt{1 - \left(\frac{v_{l,min}}{c}\right)^2}} R_1 = \frac{m_o v_t}{\sqrt{1 - \frac{v_t^2 + v_z^2}{c^2}}} R_2 \quad (39a)$$



$$\frac{m_o v_{l,min} \sin \theta}{\sqrt{1 - \left(\frac{v_{l,min}}{c}\right)^2}} = \frac{m_o v_z}{\sqrt{1 - \frac{v_t^2 + v_z^2}{c^2}}} \quad (40a)$$

where v_r (radial velocity at the collector) is taken as zero and v_z is defined as the velocity of the beta particle in the z-direction at the collector. The equations can be solved to give

$$\frac{(U_{l,min} + U_o - e\Phi)^2 - U_o^2}{(U_{l,min} + U_o)^2 - U_o^2} = \left(\frac{R_1}{R_2}\right)^2 \cos^2 \theta \sin^2 \varphi + \sin^2 \theta \quad (41a)$$

from which $U_{l,min}$, the minimum initial kinetic energy, can be found. (The non-relativistic formulations of the equations of motion (eqs. (38a) to (40a) are:

$$\left(\frac{1}{2} m_o v_{l,min}^2\right) = \frac{1}{2} m_o (v_t^2 + v_z^2) + e\Phi \quad (38b)$$

$$m_o v_{l,min} \cos \theta \sin \varphi R_1 = m_o v_t R_2 \quad (39b)$$

$$m_0 v \sin \theta = m_0 v_z \quad (40b)$$

On eliminating v_t and v_z among them,

$$\frac{\left(\frac{1}{2} m_0 v_{1,\min}^2\right) - e\Phi}{\left(\frac{1}{2} m_0 v_{1,\min}^2\right)} = \left(\frac{R_1}{R_2}\right)^2 \cos^2 \theta \sin^2 \varphi + \sin^2 \theta \quad (41b)$$

is obtained.) Continuing to follow the procedure previously set forth (for the spherical case), the limits $r_{\max}(\theta, \varphi)$, $\theta_{\max}(\varphi)$, and $\varphi_{\max}(\theta = 0)$ can be obtained by replacing $t_s/\cos \theta$ (spherical case) by $t_s/(\cos \theta \cos \varphi)$ (cylindrical case). Sets of these limits can be produced by repetition of the generating process.

It is again necessary to modify these limits by taking into account the geometric boundaries of the fuel layer. As a result, there exists a $\theta_t(\varphi)$ that satisfies the relation

$$\left. \begin{aligned} \cos \theta_t &= \frac{t_f}{r_{\max}(\theta_t, \varphi) \cos \varphi} & \theta_t > 0 \\ 1 &\leq \frac{t_f}{r_{\max}(0, \varphi) \cos \varphi} & \theta_t = 0 \end{aligned} \right\} \quad (42)$$

and a $\varphi_t(\theta = 0)$ that satisfies the relation

$$\left. \begin{aligned} \cos \varphi_t &= \frac{t_f}{r_{\max}(0, \varphi_t)} & \varphi_t > 0 \\ 1 &\leq \frac{t_f}{r_{\max}(0, 0)} & \varphi_t = 0 \end{aligned} \right\} \quad (43)$$

Also, the values of φ_{\max} and θ_{\max} must not exceed $\pi/2$. Therefore,

$$\begin{aligned} n_e = \frac{N}{\pi} & \left(\int_0^{\varphi_t} d\varphi \int_0^{\theta_t} d\theta \int_0^{t_f/\cos \theta \cos \varphi} \cos^2 \theta \cos \varphi dr \right. \\ & + \int_0^{\varphi_t} d\varphi \int_{\theta_t}^{\theta_{\max}} d\theta \int_0^{r_{\max}} \cos^2 \theta \cos \varphi dr \\ & \left. + \int_{\varphi_t}^{\varphi_{\max}} d\varphi \int_0^{\theta_{\max}} d\theta \int_0^{r_{\max}} \cos^2 \theta \cos \varphi dr \right) \quad (44) \end{aligned}$$

which reduces to

$$n_{\epsilon} = \frac{N_{\epsilon}}{\pi} \left[t_f \int_0^{\Phi_t} \sin \theta_t d\varphi + \int_0^{\Phi_t} d\varphi \int_{\Phi_t}^{\theta_{\max}(\varphi)} r_{\max} \cos^2 \theta \cos \varphi d\theta \right. \\ \left. + \int_{\Phi_t}^{\Phi_{\max}} d\varphi \int_0^{\theta_{\max}(\varphi)} r_{\max} \cos^2 \theta \cos \varphi d\theta \right] \quad (45)$$

for beta particles of energy E_{β} . Here again both forward directed and backward directed particles are accounted for by choosing t_f as twice the actual fuel-layer thickness.

Total Energy Reaching Collector

From the discussion set forth for the spherical configuration, it can be seen that the energy per second per unit emitter area reaching the collector for the cylindrical configuration is

$$E_c = \frac{N}{\pi} \sum n(E_{\beta}) \left(\int_0^{\Phi_t} d\varphi \int_0^{\theta_t} d\theta \int_0^{t_f / \cos \theta \cos \varphi} E_{p,c} \cos^2 \theta \cos \varphi dr \right. \\ \left. + \int_0^{\Phi_t} d\varphi \int_{\theta_t}^{\theta_{\max}} d\theta \int_0^{r_{\max}} \cos^2 \theta \cos \varphi E_{p,c} dr \right. \\ \left. + \int_{\Phi_t}^{\Phi_{\max}} d\varphi \int_0^{\theta_{\max}} d\theta \int_0^{r_{\max}} \cos^2 \theta \cos \varphi E_{p,c} dr \right) \Delta E / \sum n(E_{\beta}) \Delta E \quad (46)$$

The quantity $E_{p,c}(r, \theta, \varphi)$ is determined in exactly the same manner as in the spherical case with the single change

$$\frac{t_s}{\cos \theta} \text{ (spherical case)} \rightarrow \frac{t_s}{\cos \theta \cos \varphi} \text{ (cylindrical case)}$$

Distribution of Particles at Collector

The quantity Δn_ϵ in the cylindrical configuration takes the form

$$\Delta n_\epsilon = \frac{N_\epsilon}{\pi} \cos^2 \theta \cos \varphi \Delta r \Delta \theta \Delta \varphi \quad (47)$$

deduced from the integral expression (34). The distribution $D(\theta, \varphi, r)$ obtained from Δn_ϵ can be converted, as was done in the spherical case, into the form $D(\theta, \varphi, E_{p,c})$. The angle with the normal at which the beta particles enter the collector, γ , is made up of the components θ_c and φ_c defined as

$$\tan \varphi_c \equiv \frac{v_t}{v_r} \quad (48)$$

and

$$\tan \theta_c \equiv \frac{\frac{v_z}{v_t}}{\sin \varphi_c} \quad (49)$$

By solving the equations of motion previously set forth for the cylindrical configuration (with v_r not equal to zero), the following equations are obtained:

$$\frac{1}{\sin^2 \varphi_c} = \frac{\left(\frac{R_2}{R_1}\right)^2}{\cos^2 \theta \sin^2 \varphi} \left[\frac{(U_1 + U_o - \phi e)^2 - U_o^2}{(U_1 + U_o)^2 - U_o^2} - \sin^2 \theta \right] \quad (50)$$

$$\frac{1}{\tan^2 \theta} = \frac{1}{\sin^2 \theta} \left[\frac{(U_1 + U_o - \phi e)^2 - U_o^2}{(U_1 + U_o)^2 - U_o^2} \right] - 1 \quad (51)$$

or, nonrelativistically,

$$\frac{1}{\sin^2 \varphi_c} = \frac{\left(\frac{R_2}{R_1}\right)^2}{\cos^2 \theta \sin^2 \varphi} \left(\frac{\frac{1}{2} m_o v_o^2 - e\phi}{\frac{1}{2} m_o v_o^2} - \sin^2 \theta \right) \quad (50b)$$

$$\frac{1}{\tan^2 \theta_c} = \frac{1}{\sin^2 \theta} \left(\frac{\frac{1}{2} m_o v_o^2 - e\phi}{\frac{1}{2} m_o v_o^2} - 1 \right) \quad (51b)$$

where U_1 (or $\frac{1}{2} m_O v_O^2$) is determined from

$$U_1 \text{ (or } \frac{1}{2} m_O v_O^2) = E_{p,c} + e\Phi \quad (52)$$

from which the angles φ_c and θ_c can be deduced. Thus, with

$$\cos \gamma = \cos \varphi_c \cos \theta_c \quad (53)$$

the distribution takes the form $D(\gamma, E_{p,c})$.

Efficiency of Cell

For a cell operating at a voltage Φ , the electrical efficiency can be written as

$$\eta = \frac{\Phi e n}{t_f N E'} \quad (54)$$

where n is the number of particles reaching the collector (per second), e the electron charge, t_f the actual fuel-layer thickness, N the number of beta particles emitted per unit volume (per second), and E' their average energy. The average energy of the beta particles can be deduced from

$$E' = \frac{\sum n(E_\beta) E \Delta E}{\sum n(E_\beta) \Delta E} \quad (55)$$

where only the 2.98-Mev (end-point energy) beta spectrum is considered. The expression for the efficiency (eq. (54)) is valid for both spherical and cylindrical configurations.

Computer Calculations

The computations were done with the IBM 7090 electronic computer following procedures (the relativistic equations and Katz-Penfold relations were used) as outlined in the preceding sections. The programs (one for each of the two cell geometries) consisted of three major calculations: the number of particles reaching the collector (with the associated cell efficiency included in this section), the total energy of the particles arriving at the collector, and the distribution of particles in terms of energy and incoming angle at the collector.

As an initial subordinate routine, the programs were set up to calculate

the beta spectrum weight factor $n(E_\beta)$ (eq. (1)). It was found that answers of sufficient accuracy were obtained in the first two sections of the computer programs when the beta spectrum was divided into 15 segments, since the answers changed by less than 2 percent when twice (30) the number of segments were used. For the particle distribution calculations, the beta spectrum had to be divided into at least 30 segments to obtain smooth distributions. Integrations were performed on the computer by use of Simpson's rule. Since sets such as $r_{\max}(\theta_1)$ and $E_{p,c}(r_1, \theta_1)$ could be obtained in the analysis, the use of numerical integration as performed on the computer was a convenient approach to the problem. The number of steps (in the variables r , θ , and ϕ) taken in the integration drastically affected the running time, and, therefore, a minimum number of steps, which allowed sufficient accuracy (less than 2-percent change on using half the step size), was used. The inverse of the Katz-Penfold relation ($E = f(R_p)$) was obtained through a polynomial curve fit in which terms beyond the 6th order were neglected.

DISCUSSION

Table I is presented as a summary of the results of the first two sections of the computer programs. In the table a variety of cases set apart by their different radius ratios and layer thicknesses (expressed in $\text{cm} \times 10^{-3}$) are presented for both cell geometries. The cell parameters n , η , and E_c are set down against operating voltage. The range of voltage is 0.2 to 1.8 Mev taken in 0.2-Mev steps. The third section of the computer programs, which pertain to the particle distributions at the collector, is presented in graphical form. Plots representing pertinent features of the analysis drawn from the data of the tables are presented. In addition, curves are shown that compare the results of using different forms of the physical constraints.

A discussion of cell design based on results of this analysis was presented in reference 6.

Number of Particles Reaching Collector

Curves of current (number of particles reaching the collector) against cell voltage are presented in figure 1 for different radius ratios and for both cell configurations. The significant feature of these curves is that an increase in the cell voltage corresponds to a decrease in the cell current. The curvature of these monotonic curves is entirely positive for all cylindrical cases, but a slight inverse curvature is detected in the higher radius-ratio cases of the spherical configuration (fig. 1(a)). This feature is probably the result of the form of the beta spectrum. An important aspect of these curves is that from them an operating point for the cell can be determined. In essence, an operating point is reached when the cell and the attached device have matched (equal) voltages and current.

Efficiency

Figure 2 represents curves of cell efficiency against cell voltage for

various radius ratios and for both cell configurations. In the collection of monoenergetic particles (ref. 3), the maximum occurs at approximately half of the highest obtainable voltage (corresponding to the energy of the particle considered). The effect of the beta spectrum changes this situation. The maximums in the plots occur between 0.4 and 0.9 megavolts, which is about half of the beta-particle average energy (1.31 Mev as determined from the computer). The long tails beyond 1.31 Mev are due to particles from the upper end of the beta spectrum reaching the collector. The weight per unit power output can be computed simply from the efficiency and weights of the various components.

Energy Distribution

Computations of the total energy of particles reaching the collector have been performed by using the analysis. Figure 3 presents typical curves. As the cell voltage increases, the number of particles reaching the collector rapidly diminishes, and thus the total energy also decreases.

With knowledge of the cell efficiency (percent of energy initially available leaving the cell) and the percentage of the energy reaching the collector, the portion of the energy distribution absorbed in the components of the cell can be calculated. Plots showing this distribution of energy are presented for both configurations and typical thickness (fig. 4). It is assumed in these plots that the energy of the particles that does not reach the collector and is not part of the power output of the cell is completely absorbed (after what may be multiple passes) in the emitter foil (fuel and support layer). A knowledge of the distribution of energy in an operating cell is important in determining component temperatures of the cell (see ref. 6).

Particle Distributions at Collector

Since the impingement of high-energy electrons on the collector can cause secondary effects, the study of the distribution of particles at this component is an important consideration. Particle distributions $D(r, E_{p,c})$ that represent the number of particles arriving at the collector as functions of particle energy and arrival angle have been evaluated for a single case for both configurations. From this information, two types of curves have been plotted: (1) The number of particles in an increment of energy and angle against arrival angle (midpoint) at a fixed particle energy increment was drawn and (2), the same dependent variable against particle energy (midpoint) for a fixed increment of arrival angle was also drawn. The increments of energy and angle taken were 0.1 Mev and 5° , respectively. The operating voltage is 0.6 Mev for both cases considered. The plots are proportional to $\partial^2 n / \partial E_{p,c} \partial \gamma$ (the second partial of n with respect to particle energy and arrival angle). These two types of curves are shown in figure 5.

The calculated points did not represent perfectly smooth curves. Smoothness of the distributions is a function of step size in the computer program. Running time is also a function of step size, but, because smoothness and a short running time are not compatible, a compromise was made.

Some of the features of figure 5 may now be noted. It is observed for the spherical case (figs. 5(a) to (e)) that the particles arriving with a high energy cannot have an arrival angle greater than some "cutoff" angle, which differs for different particle arrival energies. It is further noted for the spherical case that particles arriving in a fixed increment of arrival angle tend to favor a small range of energies (see figs. 5(f) to (h)). In the cylindrical case (figs. 5(i) to (o)), this bunching is not observed in either type of plot. Instead, the curves spread out over the entire range of the variables considered. The nature of the spreading is a result of the geometry, but the fact that spreading does exist is due mainly to the beta spectrum and slightly to the different origins of the beta particles in the fuel layer.

Effects of Changes in Physical Relations

Figure 6 shows an interesting comparison of cell efficiency plots for the cerium-praseodymium 2.98-Mev beta particle and a hypothetical 2.18-Mev beta particle from an allowed nuclear transition. Changing the beta spectrum not only affects the spread of the curve but also affects the value of the maximum.

Figure 7 compares the results of using the relativistic and nonrelativistic equations in a typical efficiency calculation. As would be expected, the effect of the relativistic equations becomes pronounced at high energies, but the difference between the two efficiency calculations is small at optimum cell voltage.

Figure 8 compares the Katz-Penfold range-energy relation for cerium and molybdenum (a possible support-layer material) with a linear approximation. Results of using these two different forms of the range-energy relation are compared in figure 9 for a typical efficiency calculation. The difference is seen to be quite small.

CONCLUDING REMARKS

A mathematical analysis of the beta radioisotope cell has been developed for calculations with an electronic computer. The beta radioisotope considered was cerium 144, which in the decay chain yields a beta-particle spectrum with a 2.98-Mev end-point energy. Results have been discussed and graphically illustrated.

From the results of the calculations, certain conclusions can be drawn. For a given radius ratio and component thickness, the maximum cell efficiency is significantly greater in the spherical configuration than in the corresponding cylindrical configuration. It is also observed that cell efficiency increases with radius ratio and that the optimum voltage (corresponding to maximum efficiency) also increases. In particle distributions at the collector it is found that cutoff angles exist in the spherical configuration where none are observed for the cylindrical configuration. Furthermore, it is found that for the lower arrival energies more particles are impinging on the collector with a grazing angle.

Changing the beta spectrum drastically affects the cell efficiency. The comparison of the relativistic equations with the nonrelativistic equations shows a small but increasing effect at high cell potentials. Finally, the use of a linear approximation in the range-energy relation has a small effect on the calculations.

Lewis Research Center
National Aeronautics and Space Administration
Cleveland, Ohio, July 25, 1963

APPENDIX - SYMBOLS

A	atomic mass number
C	speed of light
$D(r, E_{p,c})$	distribution at collector
E	energy
E_c	total energy arriving at collector
E_f	energy lost in fuel layer
E_o	end-point energy
$E_{p,c}$	energy of beta particle at collector
E_s	energy lost in support layer
E_β	energy of emitted beta particle
e	electronic charge
m_o	mass of electron
N	number of disintegrations per unit volume per second
n	number of particles per unit emitter area per second reaching collector
$n(E_\beta)$	relative number of particles in beta spectrum
$n^*(E_\beta)$	normalized $n(E_\beta)$
P_t	linear tangential momentum
P_z	linear momentum in z-direction
R_p	practical range; effective straight-line distance in which an electron loses its entire initial energy
R_1	inner radius
R_2	outer radius
r	radial distance
dr	differential element of radial distance

r_{\max}	maximum radial distance
dS	differential element of surface area
t_f	fuel-layer thickness
t_s	support-layer thickness
U	kinetic energy of beta particle
U_0	rest mass energy
U_1	kinetic energy of beta particle emitter
U_2	kinetic energy of beta particle collector
V	operating voltage, Mev
v	velocity
v_z	velocity of beta particle in z-direction at collector
Z	atomic number
γ	arrival angle (normal) at collector
ϵ	defined in eq. (1)
η	cell efficiency
θ	polar angle
θ_c	θ -component of arrival angle
θ_{\max}	maximum polar angle
dv	differential element of volume
Φ	cell voltage
φ	azimuthal angle
φ_c	φ -component of arrival angle
φ_{\max}	maximum azimuthal angle
Superscript	
'	times a unit area

Subscripts:

max maximum

min minimum

p projected area

ϵ in an increment of energy

1 initial (emitter)

2 final (collector)

REFERENCES

1. Low, Charles A., Jr., and Mickelsen, William R.: An Electrostatic Propulsion System with a Direct Nuclear Electrogenerator. Paper Presented at IAS Nat. Prop. Meeting, Cleveland (Ohio), Mar. 9, 1962. (See also Aerospace Eng., vol. 21, no. 1, Dec. 1962, pp. 58-59; 72-87.)
2. Mickelsen, William R.: NASA Research on Heavy-Particle Electrostatic Thrustors. Paper 63-19, Inst. Aero. Sci., 1963.
3. Heindl, Clifford J.: Efficiency of Fission Electric Cells. Tech. Rep. 32-105, Jet Prop. Lab., C.I.T., May 1961.
4. Schock, Alfred: A Direct Nuclear Electrogenerator. Analysis of Cylindrical Electrode Configuration. AFOSR TN 59-590, Fairchild Engine Div., June 15, 1959.
5. Mickelsen, W. R., and Low, C. A.: Potentialities of the Radioisotope Electrostatic Propulsion System. Paper 63048A, AIAA, 1963.
6. Cohen, Allan J., and Low, Charles A.: A Parametric Study of Direct Nuclear Electrogenerator Cells Using a Beta Emitting Source. Paper 63048B, AIAA, 1963.
7. Bethe, H. A., and Morrison, P. M.: Elementary Nuclear Theory. John Wiley & Sons, Inc., 1956.
8. Graham, R. L., Geiger, J. S., and Eastwood, T. A.: Experimental Evidence for Axial Vector Interaction in the Disintegration of Pr-144. Canadian Jour. Phys., vol. 36, July-Dec. 1958, pp. 1084-1111.
9. Katz, L., and Penfold, A. S.: Range-Energy Relations for Electrons and Determination of Beta-Ray End-Point Energies by Absorption. Rev. Modern Phys., vol. 24, no. 1, Jan. 1952, pp. 28-44.
10. Glendenin, Lawrence E.: Determination of the Energy of Beta Particles and Photons by Absorption. Nucleonics, vol. 2, Jan. 1948, pp. 12-32.

TABLE I. - COMPUTER OUTPUT FOR CERIUM 144 CELL WITH MOLYBDENUM SUPPORT LAYER

(a) Spherical configuration

Fuel-layer thickness, t_f , cm							
1.27×10^{-3}				2.54×10^{-3}			
Support-layer thickness, t_s , cm							
2.54×10^{-3}				2.54×10^{-3}			
Radius ratio, R_2/R_1							
2.0				2.0			
Cell voltage, Φ , mega-volts	Number of particles, n , percent	Cell efficiency, η , percent	Total energy arriving at collector, E_c , percent	Cell voltage, Φ , mega-volts	Number of particles, n , percent	Cell efficiency, η , percent	Total energy arriving at collector, E_c , percent
0.2	83.8	12.8	66.8	0.2	82.1	12.5	64.4
.4	74.9	22.9	53.9	.4	73.2	22.3	51.8
.6	62.6	28.6	41.5	.6	61.2	28.0	39.8
.8	48.6	29.7	30.1	.8	47.1	28.8	28.9
1.0	33.9	25.9	20.2	1.0	32.4	24.8	19.1
1.2	21.5	19.7	12.0	1.2	20.3	18.6	11.2
1.4	11.4	12.2	5.85	1.4	11.1	11.9	5.53
1.6	5.80	7.09	2.50	1.6	5.81	7.10	2.43
1.8	2.72	3.74	.96	1.8	2.73	3.75	.93
Fuel-layer thickness, t_f , cm							
5.08×10^{-3}				5.08×10^{-3}			
Support-layer thickness, t_s , cm							
2.54×10^{-3}				2.54×10^{-3}			
Radius ratio, R_2/R_1							
1.1				1.3			
Cell voltage, Φ , mega-volts	Number of particles, n , percent	Cell efficiency, η , percent	Total energy arriving at collector, E_c , percent	Cell voltage, Φ , mega-volts	Number of particles, n , percent	Cell efficiency, η , percent	Total energy arriving at collector, E_c , percent
0.2	58.6	8.95	51.8	0.2	73.5	11.2	59.2
.4	35.0	10.7	28.9	.4	53.6	16.3	43.1
.6	22.0	10.1	16.5	.6	34.2	15.6	26.1
.8	14.0	8.55	9.60	.8	20.8	12.7	14.2
1.0	8.64	6.59	5.30	1.0	12.7	9.70	7.85
1.2	5.07	4.65	2.76	1.2	7.40	6.77	4.07
1.4	2.66	2.84	1.25	1.4	4.02	4.29	1.95
1.6	1.48	1.80	.61	1.6	2.12	2.60	.86
1.8	.61	.84	.20	1.8	.94	1.29	.23

TABLE I. - Continued. COMPUTER OUTPUT FOR CERIUM 144 CELL
WITH MOLYBDENUM SUPPORT LAYER

(a) Continued. Spherical configuration

Fuel-layer thickness, t_f , cm							
5.08×10^{-3}				5.08×10^{-3}			
Support-layer thickness, t_s , cm							
2.54×10^{-3}				2.54×10^{-3}			
Radius ratio, R_2/R_1							
1.5				1.8			
Cell voltage, ϕ , mega-volts	Number of particles, n , percent	Cell efficiency, η , percent	Total energy arriving at collector, E_c , percent	Cell voltage, ϕ , mega-volts	Number of particles, n , percent	Cell efficiency, η , percent	Total energy arriving at collector, E_c , percent
0.2	75.5	11.5	59.6	0.2	78.3	11.9	60.0
.4	62.0	18.9	43.4	.4	66.9	20.4	47.6
.6	45.5	20.8	32.9	.6	54.2	24.8	36.0
.8	29.3	17.8	20.2	.8	39.2	23.9	25.0
1.0	17.7	13.5	11.0	1.0	25.6	19.6	15.5
1.2	10.1	9.22	5.55	1.2	15.1	13.8	8.40
1.4	5.41	5.78	2.62	1.4	8.20	8.77	3.95
1.6	2.83	3.45	1.13	1.6	4.18	5.10	1.70
1.8	1.33	1.83	.46	1.8	1.92	2.65	.64
Fuel-layer thickness, t_f , cm							
5.08×10^{-3}				5.08×10^{-3}			
Support-layer thickness, t_s , cm							
2.54×10^{-3}				2.54×10^{-3}			
Radius ratio, R_2/R_1							
2.0				4.0			
Cell voltage, ϕ , mega-volts	Number of particles, n , percent	Cell efficiency, η , percent	Total energy arriving at collector, E_c , percent	Cell voltage, ϕ , mega-volts	Number of particles, n , percent	Cell efficiency, η , percent	Total energy arriving at collector, E_c , percent
0.2	78.6	12.0	60.0	0.2	79.4	12.1	60.0
.4	68.8	21.0	47.9	.4	72.0	22.0	48.2
.6	57.0	26.0	36.6	.6	63.7	29.2	37.4
.8	43.2	26.4	26.2	.8	54.0	32.9	27.9
1.0	30.0	22.9	17.3	1.0	43.2	32.9	20.0
1.2	18.5	16.9	9.96	1.2	32.4	29.7	13.6
1.4	10.3	10.9	4.96	1.4	22.4	23.9	8.46
1.6	5.29	6.46	2.16	1.6	14.0	17.2	4.70
1.8	2.44	3.34	.80	1.8	7.96	10.9	2.25

TABLE I. - Continued. COMPUTER OUTPUT FOR CERTUM 144 CELL

WITH MOLYBDENUM SUPPORT LAYER

(a) Continued. Spherical configuration

Fuel-layer thickness, t_f , cm							
5.08×10^{-3}				5.08×10^{-3}			
Support-layer thickness, t_s , cm							
2.54×10^{-3}				1.27×10^{-3}			
Radius ratio, R_2/R_1							
10.0				1.5			
Cell voltage, Φ , mega-volts	Number of particles, n , percent	Cell efficiency, η , percent	Total energy arriving at collector, E_c , percent	Cell voltage, Φ , mega-volts	Number of particles, n , percent	Cell efficiency, η , percent	Total energy arriving at collector, E_c , percent
0.2	79.5	12.1	60.0	0.2	78.9	12.0	63.7
.4	72.7	22.2	48.2	.4	65.1	19.7	50.0
.6	65.5	30.0	37.5	.6	47.5	21.8	35.6
.8	56.5	34.5	28.1	.8	30.9	18.8	21.9
1.0	46.6	35.6	20.0	1.0	18.5	14.1	11.9
1.2	36.3	33.2	13.8	1.2	10.5	9.62	5.89
1.4	26.4	28.2	8.81	1.4	5.88	6.28	2.89
1.6	18.0	22.0	5.09	1.6	3.06	3.74	1.26
1.8	11.4	15.6	2.54	1.8	1.45	1.99	.49
Fuel-layer thickness, t_f , cm							
5.08×10^{-3}				5.08×10^{-3}			
Support-layer thickness, t_s , cm							
1.27×10^{-3}				1.27×10^{-3}			
Radius ratio, R_2/R_1							
2.0				4.0			
Cell voltage, Φ , mega-volts	Number of particles, n , percent	Cell efficiency, η , percent	Total energy arriving at collector, E_c , percent	Cell voltage, Φ , mega-volts	Number of particles, n , percent	Cell efficiency, η , percent	Total energy arriving at collector, E_c , percent
0.2	80.9	12.4	64.0	0.2	82.2	12.5	64.0
.4	72.0	22.0	51.5	.4	75.3	23.0	51.7
.6	59.9	27.4	39.6	.6	66.7	30.5	40.4
.8	45.9	28.0	28.7	.8	57.0	34.8	30.4
1.0	31.6	24.1	18.9	1.0	46.4	35.4	22.0
1.2	19.9	18.2	11.0	1.2	34.5	31.6	15.1
1.4	11.3	12.0	5.58	1.4	24.2	25.8	9.51
1.6	5.67	6.92	2.37	1.6	15.5	18.9	5.38
1.8	2.70	3.71	.92	1.8	8.88	12.2	2.62

TABLE 1. - Continued. COMPUTER OUTPUT FOR CERIUM 144 CELL

WITH MOLYBDENUM SUPPORT LAYER

(a) Continued. Spherical configuration

Fuel-layer thickness, t_f , cm							
5.08×10^{-3}				5.08×10^{-3}			
Support-layer thickness, t_s , cm							
5.08×10^{-3}				5.08×10^{-3}			
Radius ratio, R_2/R_1							
1.5				2.0			
Cell voltage, Φ , mega-volts	Number of particles, n , percent	Cell efficiency, η , percent	Total energy arriving at collector, E_c , percent	Cell voltage, Φ , mega-volts	Number of particles, n , percent	Cell efficiency, η , percent	Total energy arriving at collector, E_c , percent
0.2	33.3	5.08	20.5	0.2	72.1	11.0	53.0
.4	25.8	7.88	14.7	.4	63.3	19.3	42.8
.6	18.1	8.30	9.52	.6	51.7	23.7	31.7
.8	11.5	7.04	5.47	.8	39.9	23.7	22.6
1.0	6.78	5.17	2.91	1.0	26.4	20.4	14.6
1.2	3.74	3.43	1.30	1.2	16.2	14.8	8.28
1.4	1.94	2.07	.56	1.4	9.03	9.65	4.12
1.6	.90	1.10	.21	1.6	4.66	5.70	1.78
1.8	.38	.53	.06	1.8	2.10	2.88	.66
Fuel-layer thickness, t_f , cm							
5.08×10^{-3}				10.16×10^{-3}			
Support-layer thickness, t_s , cm							
10.16×10^{-3}				2.54×10^{-3}			
Radius ratio, R_2/R_1							
2.0				2.0			
Cell voltage, Φ , mega-volts	Number of particles, n , percent	Cell efficiency, η , percent	Total energy arriving at collector, E_c , percent	Cell voltage, Φ , mega-volts	Number of particles, n , percent	Cell efficiency, η , percent	Total energy arriving at collector, E_c , percent
0.2	62.8	9.59	42.5	0.2	70.3	10.7	52.4
.4	53.9	16.4	33.0	.4	60.8	18.5	41.4
.6	43.8	19.8	24.3	.6	50.0	22.9	31.2
.8	31.4	19.2	16.7	.8	37.6	29.9	22.0
1.0	20.8	15.8	10.4	1.0	25.7	19.6	14.2
1.2	12.5	11.5	5.82	1.2	15.8	14.5	8.06
1.4	6.89	7.36	2.79	1.4	8.82	9.43	3.96
1.6	3.43	4.19	1.15	1.6	4.57	5.53	1.72
1.8	1.52	2.09	.40	1.8	2.12	2.92	.64

TABLE I. - Continued. COMPUTER OUTPUT FOR CERIUM 144 CELL

WITH MOLYBDENUM SUPPORT LAYER

(a) Continued. Spherical configuration

Fuel-layer thickness, t_f , cm							
12.7×10 ⁻³				20.24×10 ⁻³			
Support-layer thickness, t_s , cm							
5.08×10 ⁻³				2.54×10 ⁻³			
Radius ratio, R_2/R_1							
2.0				2.0			
Cell voltage, Φ , mega-volts	Number of particles, n , percent	Cell efficiency, η , percent	Total energy arriving at collector, E_c , percent	Cell voltage, Φ , mega-volts	Number of particles, n , percent	Cell efficiency, η , percent	Total energy arriving at collector, E_c , percent
0.2	62.2	9.50	43.9	0.2	58.1	8.87	41.4
.4	53.6	16.8	34.2	.4	50.0	15.3	32.1
.6	43.3	19.8	25.4	.6	40.3	18.5	23.7
.8	31.9	19.5	17.5	.8	30.0	18.3	16.3
1.0	21.3	16.2	11.0	1.0	20.0	15.2	10.2
1.2	13.0	11.9	6.10	1.2	12.2	11.2	5.64
1.4	7.22	7.72	2.96	1.4	6.75	7.21	2.72
1.6	3.64	4.45	1.23	1.6	3.42	4.17	1.11
1.8	1.64	2.25	.44	1.8	1.55	2.14	.39
Fuel-layer thickness, t_f , cm							
28.4×10 ⁻³				40.64×10 ⁻³			
Support-layer thickness, t_s , cm							
5.08×10 ⁻³				2.54×10 ⁻³			
Radius ratio, R_2/R_1							
2.0				2.0			
Cell voltage, Φ , mega-volts	Number of particles, n , percent	Cell efficiency, η , percent	Total energy arriving at collector, E_c , percent	Cell voltage, Φ , mega-volts	Number of particles, n , percent	Cell efficiency, η , percent	Total energy arriving at collector, E_c , percent
0.2	49.9	7.62	33.2	0.2	42.3	6.46	27.6
.4	42.2	13.0	25.2	.4	35.5	10.8	20.8
.6	33.5	15.3	18.2	.6	28.0	12.8	14.8
.8	24.3	14.8	12.3	.8	20.3	12.4	9.91
1.0	16.0	12.2	7.47	1.0	13.4	10.2	5.98
1.2	9.50	8.70	3.97	1.2	7.99	7.32	3.18
1.4	5.12	5.54	1.87	1.4	4.32	4.61	1.46
1.6	2.58	3.15	.74	1.6	2.13	2.60	.57
1.8	1.13	1.55	.25	1.8	.93	1.28	.20

TABLE I. - Continued. COMPUTER OUTPUT FOR CERIUM 144 CELL

WITH MOLYBDENUM SUPPORT LAYER

(a) Concluded. Spherical configuration

Fuel-layer thickness, t_f , cm							
101.6 $\times 10^{-3}$				0.127 $\times 10^{-3}$			
Support-layer thickness, t_s , cm							
5.08 $\times 10^{-3}$				2.54 $\times 10^{-3}$			
Radius ratio, R_2/R_1							
1.5				2.0			
Cell voltage, Φ , mega-volts	Number of particles, n , percent	Cell ef- ficiency, η , percent	Total energy arriving at col- lector, E_c , percent	Cell voltage, Φ , mega- volts	Number of particles, n , percent	Cell ef- ficiency, η , percent	Total energy arriving at col- lector, E_c , percent
0.2	18.6	2.83	10.5	0.2	84.3	12.7	69.1
.4	14.2	4.34	7.39	.4	75.7	23.1	55.8
.6	9.84	4.50	4.70	.6	63.5	29.1	43.1
.8	6.17	3.77	2.66	.8	48.7	29.7	31.1
1.0	3.57	2.72	1.33	1.0	34.3	26.2	20.1
1.2	1.93	1.76	.68	1.2	21.5	19.7	12.4
1.4	.97	1.04	.26	1.4	11.5	12.3	5.99
1.6	.45	.55	.09	1.6	5.80	7.09	2.57
1.8	.19	.26	.03	1.8	2.72	3.74	.99

TABLE I. - Continued. COMPUTER OUTPUT FOR CERIUM 144 CELL

WITH MOLYBDENUM SUPPORT LAYER

(b) Cylindrical configuration

Fuel-layer thickness, t_f , cm							
1.27×10^{-3}				2.54×10^{-3}			
Support-layer thickness, t_s , cm							
2.54×10^{-3}				2.54×10^{-3}			
Radius ratio, R_2/R_1							
2.0				2.0			
Cell voltage, Φ , mega-volts	Number of particles, n , percent	Cell efficiency, η , percent	Total energy arriving at collector, E_c , percent	Cell voltage, Φ , mega-volts	Number of particles, n , percent	Cell efficiency, η , percent	Total energy arriving at collector, E_c , percent
0.2	68.1	10.4	58.4	0.2	67.3	10.2	57.0
.4	51.6	15.7	40.6	.4	50.8	15.5	39.8
.6	37.1	16.9	26.9	.6	36.8	16.8	26.6
.8	25.8	15.7	16.6	.8	25.0	15.2	16.6
1.0	16.8	12.8	9.59	1.0	15.9	12.1	9.53
1.2	9.83	8.97	5.10	1.2	9.22	8.42	5.04
1.4	5.01	5.33	2.42	1.4	4.83	5.15	2.36
1.6	2.32	2.83	1.00	1.6	2.35	2.86	.98
1.8	1.02	1.40	.37	1.8	1.04	1.42	.37
Fuel-layer thickness, t_f , cm							
5.08×10^{-3}				5.08×10^{-3}			
Support-layer thickness, t_s , cm							
2.54×10^{-3}				2.54×10^{-3}			
Radius ratio, R_2/R_1							
1.1				1.3			
Cell voltage, Φ , mega-volts	Number of particles, n , percent	Cell efficiency, η , percent	Total energy arriving at collector, E_c , percent	Cell voltage, Φ , mega-volts	Number of particles, n , percent	Cell efficiency, η , percent	Total energy arriving at collector, E_c , percent
0.2	51.4	7.82	44.8	0.2	59.6	9.07	50.0
.4	30.5	9.28	24.8	.4	39.4	12.0	31.6
.6	19.2	8.77	14.2	.6	24.2	11.1	18.2
.8	11.9	7.29	8.04	.8	14.7	8.93	9.92
1.0	7.24	5.50	4.39	1.0	8.77	6.67	5.31
1.2	4.18	3.81	2.26	1.2	4.95	4.52	2.71
1.4	2.23	2.38	1.06	1.4	2.86	3.04	1.32
1.6	1.22	1.48	.48	1.6	1.47	1.80	.57
1.8	.50	.67	.17	1.8	.64	.88	.21

TABLE I. - Continued. COMPUTER OUTPUT FOR CERIUM 144 CELL

WITH MOLYBDENUM SUPPORT LAYER

(b) Continued. Cylindrical configuration

Fuel-layer thickness, t_f , cm							
5.08×10 ⁻³				5.08×10 ⁻³			
Support-layer thickness, t_s , cm							
2.54×10 ⁻³				2.54×10 ⁻³			
Radius ratio, R_2/R_1							
1.5				1.8			
Cell voltage, ϕ , mega-volts	Number of particles, n , percent	Cell efficiency, η , percent	Total energy arriving at collector, E_c , percent	Cell voltage, ϕ , mega-volts	Number of particles, n , percent	Cell efficiency, η , percent	Total energy arriving at collector, E_c , percent
0.2	62.5	9.51	51.5	0.2	64.5	9.82	52.4
.4	44.3	13.5	34.3	.4	47.9	14.6	36.1
.6	29.3	13.4	21.3	.6	33.9	15.5	23.6
.8	17.9	10.9	12.2	.8	22.2	13.5	14.3
1.0	10.4	7.93	6.34	1.0	13.6	10.4	8.12
1.2	5.91	5.39	3.21	1.2	7.49	6.84	4.08
1.4	3.33	3.55	1.55	1.4	3.96	4.22	1.86
1.6	1.63	1.99	.65	1.6	2.04	2.48	.78
1.8	.78	1.06	.25	1.8	.84	1.14	.26
Fuel-layer thickness, t_f , cm							
5.08×10 ⁻³				5.08×10 ⁻³			
Support-layer thickness, t_s , cm							
2.54×10 ⁻³				2.54×10 ⁻³			
Radius ratio, R_2/R_1							
2.0				4.0			
Cell voltage, ϕ , mega-volts	Number of particles, n , percent	Cell efficiency, η , percent	Total energy arriving at collector, E_c , percent	Cell voltage, ϕ , mega-volts	Number of particles, n , percent	Cell efficiency, η , percent	Total energy arriving at collector, E_c , percent
0.2	65.1	9.91	52.7	0.2	66.9	10.2	53.5
.4	49.1	14.9	36.6	.4	52.4	16.0	38.0
.6	35.4	16.1	24.3	.6	40.0	18.2	26.1
.8	23.9	14.5	15.1	.8	29.2	17.7	17.0
1.0	15.2	11.6	8.78	1.0	20.2	15.4	10.6
1.2	8.68	7.93	4.65	1.2	13.6	12.3	6.20
1.4	4.62	4.93	2.15	1.4	8.52	9.07	3.34
1.6	2.23	2.72	.86	1.6	4.72	5.75	1.58
1.8	.97	1.32	.30	1.8	2.12	2.99	.63

TABLE I. - Continued. COMPUTER OUTPUT FOR CERIUM 144 CELL
WITH MOLYBDENUM SUPPORT LAYER
(b) Continued. Cylindrical configuration

Fuel-layer thickness, t_f , cm							
5.08×10^{-3}				5.08×10^{-3}			
Support-layer thickness, t_s , cm							
2.54×10^{-3}				1.27×10^{-3}			
Radius ratio, R_2/R_1							
10.0				1.5			
Cell voltage, ϕ , mega-volts	Number of particles, n , percent	Cell efficiency, η , percent	Total energy arriving at collector, E_c , percent	Cell voltage, ϕ , mega-volts	Number of particles, n , percent	Cell efficiency, η , percent	Total energy arriving at collector, E_c , percent
0.2	67.4	10.3	53.8	0.2	64.7	9.85	55.0
.4	53.1	16.2	38.3	.4	46.2	14.1	37.0
.6	40.9	18.7	26.4	.6	30.5	13.9	23.2
.8	30.4	18.5	17.4	.8	19.0	11.5	13.7
1.0	21.8	16.5	10.9	1.0	11.0	8.38	6.87
1.2	14.7	13.4	6.53	1.2	6.25	5.70	3.46
1.4	9.76	10.4	3.62	1.4	3.42	3.63	1.65
1.6	5.95	7.24	1.79	1.6	1.72	2.09	.70
1.8	3.12	4.38	.75	1.8	.79	1.08	.27
Fuel-layer thickness, t_f , cm							
5.08×10^{-3}				5.08×10^{-3}			
Support-layer thickness, t_s , cm							
1.27×10^{-3}				1.27×10^{-3}			
Radius ratio, R_2/R_1							
2.0				4.0			
Cell voltage, ϕ , mega-volts	Number of particles, n , percent	Cell efficiency, η , percent	Total energy arriving at collector, E_c , percent	Cell voltage, ϕ , mega-volts	Number of particles, n , percent	Cell efficiency, η , percent	Total energy arriving at collector, E_c , percent
0.2	67.2	10.2	56.3	0.2	69.1	10.5	57.2
.4	51.0	15.5	39.5	.4	54.3	16.5	40.9
.6	37.0	16.9	26.4	.6	41.6	19.0	28.3
.8	25.4	15.5	16.7	.8	30.8	18.7	18.8
1.0	15.9	12.1	9.87	1.0	21.7	16.5	11.8
1.2	9.31	8.50	5.30	1.2	14.3	13.1	7.08
1.4	5.01	5.33	2.46	1.4	9.03	9.62	3.91
1.6	2.42	2.95	.99	1.6	5.18	6.30	1.91
1.8	1.11	1.52	.37	1.8	2.57	3.53	.77

TABLE I. - Continued. COMPUTER OUTPUT FOR CERIUM 144 CELL
WITH MOLYBDENUM SUPPORT LAYER

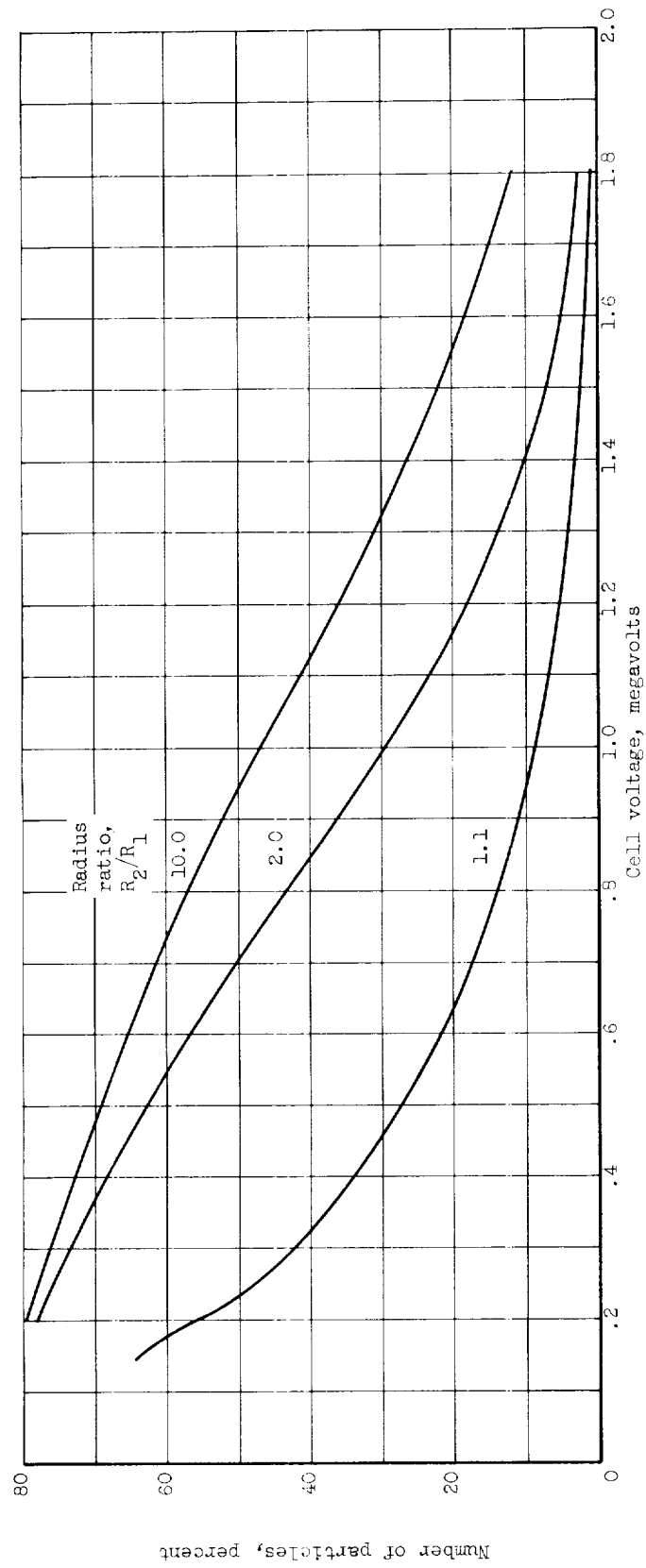
(b) Continued. Cylindrical configuration

Fuel-layer thickness, t_f , cm							
5.08×10^{-3}				5.08×10^{-3}			
Support-layer thickness, t_s , cm							
5.08×10^{-3}				5.08×10^{-3}			
Radius ratio, R_2/R_1							
1.5				2.0			
Cell voltage, ϕ , mega-volts	Number of particles, n , percent	Cell efficiency, η , percent	Total energy arriving at collector, E_c , percent	Cell voltage, ϕ , mega-volts	Number of particles, n , percent	Cell efficiency, η , percent	Total energy arriving at collector, E_c , percent
0.2	29.3	4.46	17.7	0.2	60.7	9.24	47.0
.4	19.8	6.02	11.2	.4	45.6	13.9	32.4
.6	12.5	5.70	6.52	.6	32.4	14.7	21.2
.8	7.35	4.47	3.45	.8	21.4	13.1	13.0
1.0	4.07	3.10	1.68	1.0	13.2	10.0	7.37
1.2	2.13	1.95	.76	1.2	7.50	6.85	3.83
1.4	1.03	1.10	.30	1.4	4.04	4.30	1.81
1.6	.45	.55	.11	1.6	1.98	2.41	.75
1.8	.17	.24	.03	1.8	.82	1.13	.25
Fuel-layer thickness, t_f , cm							
5.08×10^{-3}				10.16×10^{-3}			
Support-layer thickness, t_s , cm							
10.16×10^{-3}				2.54×10^{-3}			
Radius ratio, R_2/R_1							
2.0				2.0			
Cell voltage, ϕ , mega-volts	Number of particles, n , percent	Cell efficiency, η , percent	Total energy arriving at collector, E_c , percent	Cell voltage, ϕ , mega-volts	Number of particles, n , percent	Cell efficiency, η , percent	Total energy arriving at collector, E_c , percent
0.2	52.8	8.03	38.2	0.2	60.4	9.18	46.4
.4	38.8	11.7	25.9	.4	45.1	13.7	32.0
.6	26.8	12.2	16.6	.6	32.2	14.6	20.9
.8	17.4	10.6	10.0	.8	21.7	13.2	12.9
1.0	10.7	8.14	5.59	1.0	13.4	10.2	7.31
1.2	5.87	5.36	2.77	1.2	7.73	7.06	3.81
1.4	3.13	3.33	1.27	1.4	4.18	4.45	1.79
1.6	1.52	1.85	.51	1.6	2.06	2.50	.75
1.8	.62	.84	.16	1.8	.91	1.25	.27

TABLE I. - Concluded. COMPUTER OUTPUT FOR CERIUM 144 CELL
WITH MOLYBDENUM SUPPORT LAYER

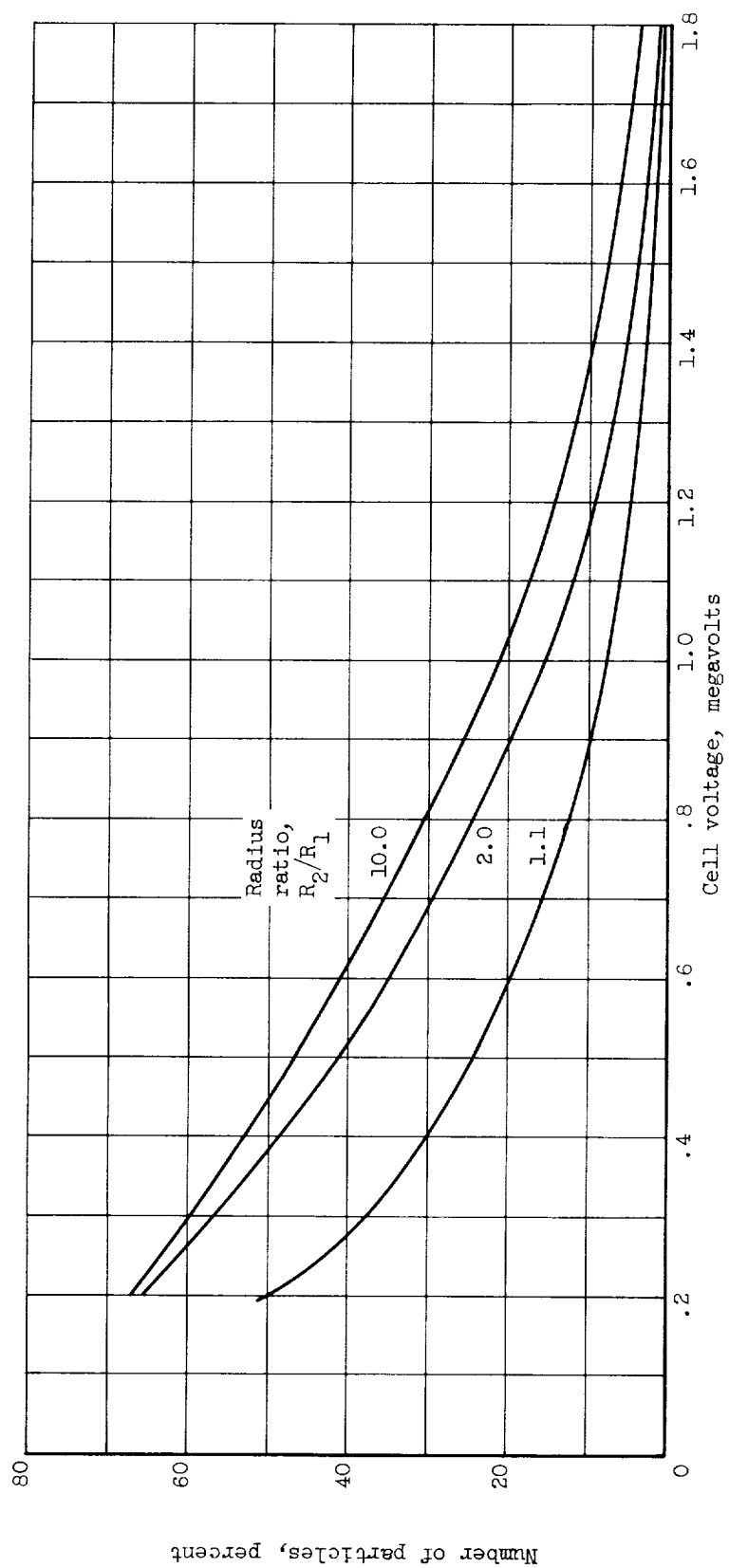
(b) Concluded. Cylindrical configuration

Fuel-layer thickness, t_f , cm							
12.7×10 ⁻³				20.24×10 ⁻³			
Support-layer thickness, t_s , cm							
5.08×10 ⁻³				2.54×10 ⁻³			
Radius ratio, R_2/R_1							
2.0				2.0			
Cell voltage, Φ , mega-volts	Number of particles, n , percent	Cell efficiency, η , percent	Total energy arriving at collector, E_c , percent	Cell voltage, Φ , mega-volts	Number of particles, n , percent	Cell efficiency, η , percent	Total energy arriving at collector, E_c , percent
0.2	54.1	8.23	39.2	0.2	51.5	7.84	36.8
.4	40.1	12.2	26.8	.4	37.9	11.5	25.1
.6	28.2	12.8	17.4	.6	26.6	12.1	16.3
.8	18.5	11.2	10.5	.8	17.5	10.6	9.75
1.0	11.3	8.63	5.90	1.0	10.7	8.15	5.45
1.2	6.51	5.94	3.00	1.2	6.10	5.57	2.77
1.4	3.41	3.63	1.40	1.4	3.18	3.39	1.24
1.6	1.67	2.03	.56	1.6	1.51	1.84	.49
1.8	.69	.95	.18	1.8	.64	.87	.16
Fuel-layer thickness, t_f , cm							
25.4×10 ⁻³				40.64×10 ⁻³			
Support-layer thickness, t_s , cm							
5.08×10 ⁻³				2.54×10 ⁻³			
Radius ratio, R_2/R_1							
2.0				2.0			
Cell voltage, Φ , mega-volts	Number of particles, n , percent	Cell efficiency, η , percent	Total energy arriving at collector, E_c , percent	Cell voltage, Φ , mega-volts	Number of particles, n , percent	Cell efficiency, η , percent	Total energy arriving at collector, E_c , percent
0.2	44.4	6.75	29.7	0.2	37.9	5.77	24.3
.4	32.3	9.83	20.0	.4	27.3	8.30	16.2
.6	22.2	10.2	12.7	.6	18.6	8.52	10.2
.8	14.3	8.72	7.51	.8	11.9	7.26	5.94
1.0	8.60	6.54	4.08	1.0	7.07	5.37	3.17
1.2	4.77	4.36	2.00	1.2	3.85	3.52	1.52
1.4	2.45	2.61	.89	1.4	1.93	2.06	.65
1.6	1.14	1.38	.33	1.6	.87	1.06	.24
1.8	.45	.62	.10	1.8	.34	.47	.07



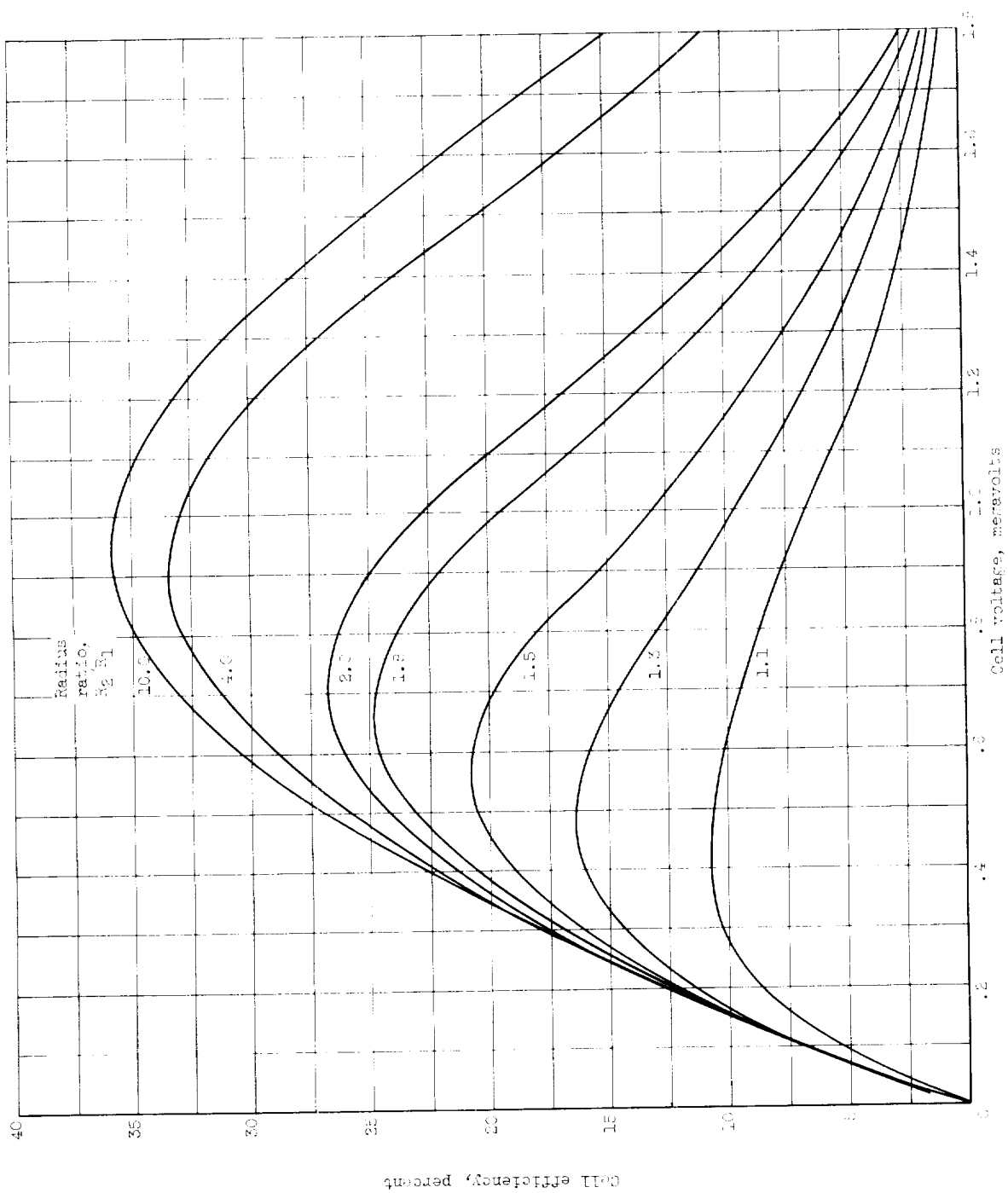
(a) Spherical configuration.

Figure 1. - Number of particles reaching collector as a function of cell voltage. Fuel-layer thickness, 35.0 milligrams per square centimeter; support-layer thickness, 25.8 milligrams per square centimeter.



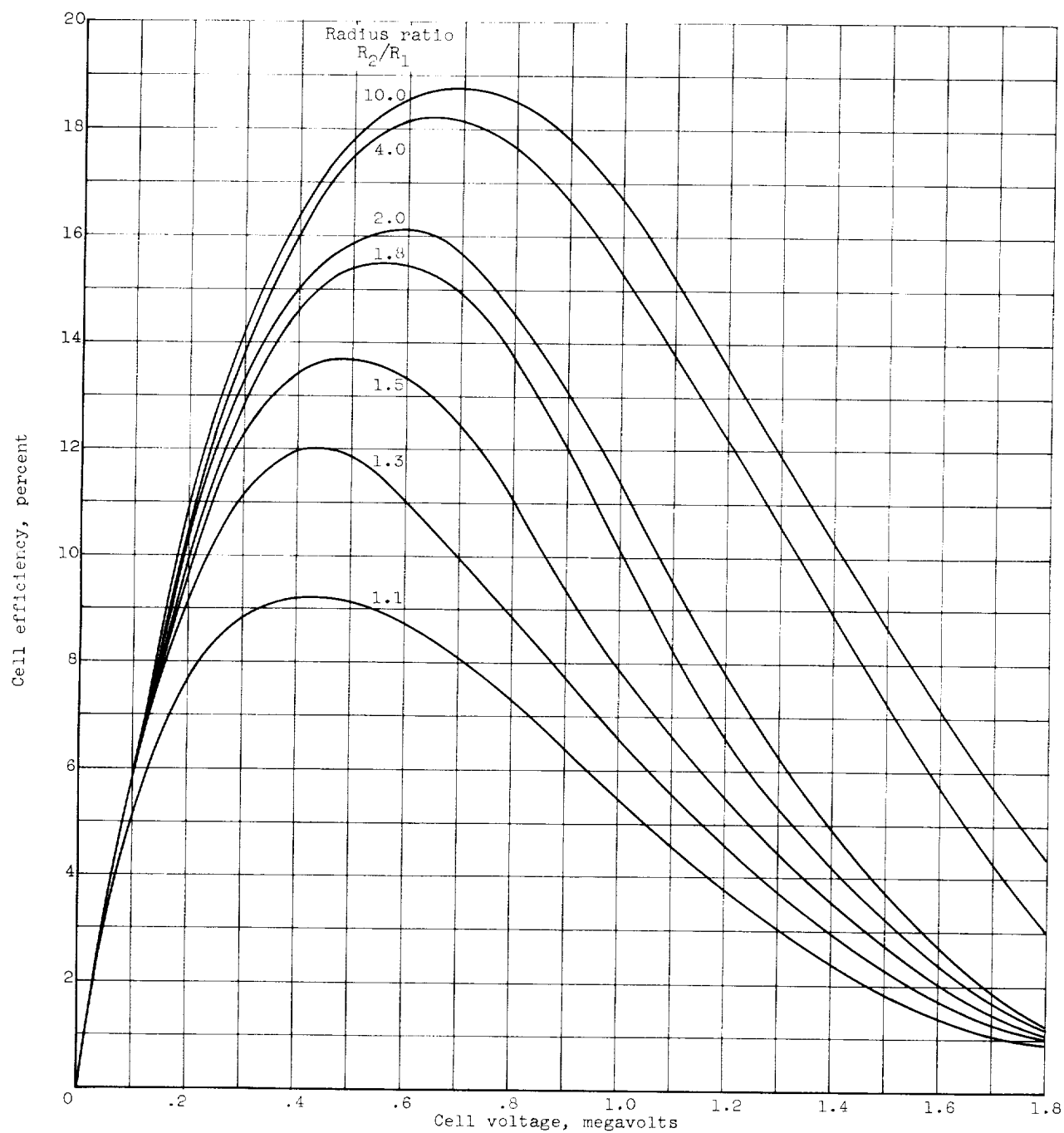
(b) Cylindrical configuration.

Figure 1. - Concluded. Number of particles reaching collector as a function of cell voltage. Fuel-layer thickness, 35.0 milligrams per square centimeter; support-layer thickness, 25.9 milligrams per square centimeter.



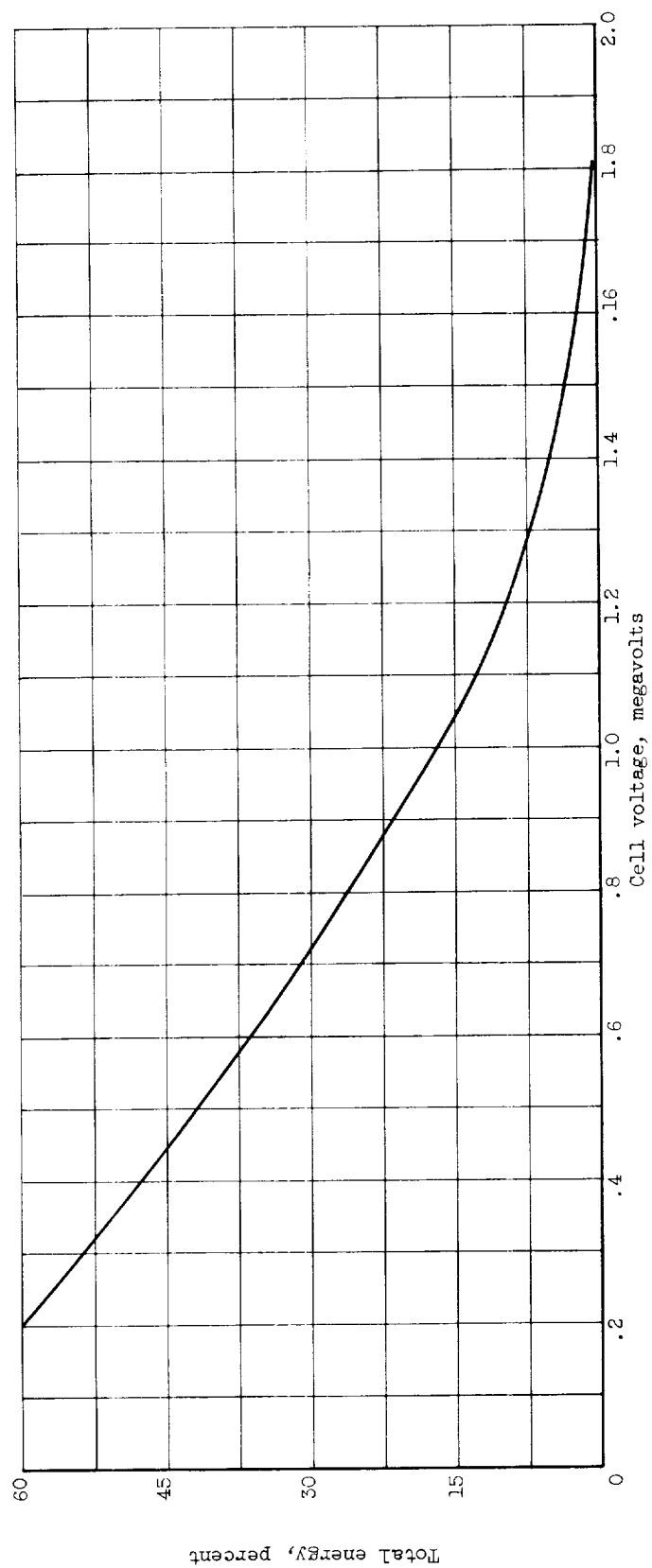
(a) Spherical configuration.

Figure 2. - Cell efficiency as a function of cell voltage for various radius ratios. Fuel-layer thickness, 25.0 milligrams per square centimeter; support-layer thickness, 25.0 milligrams per square centimeter.



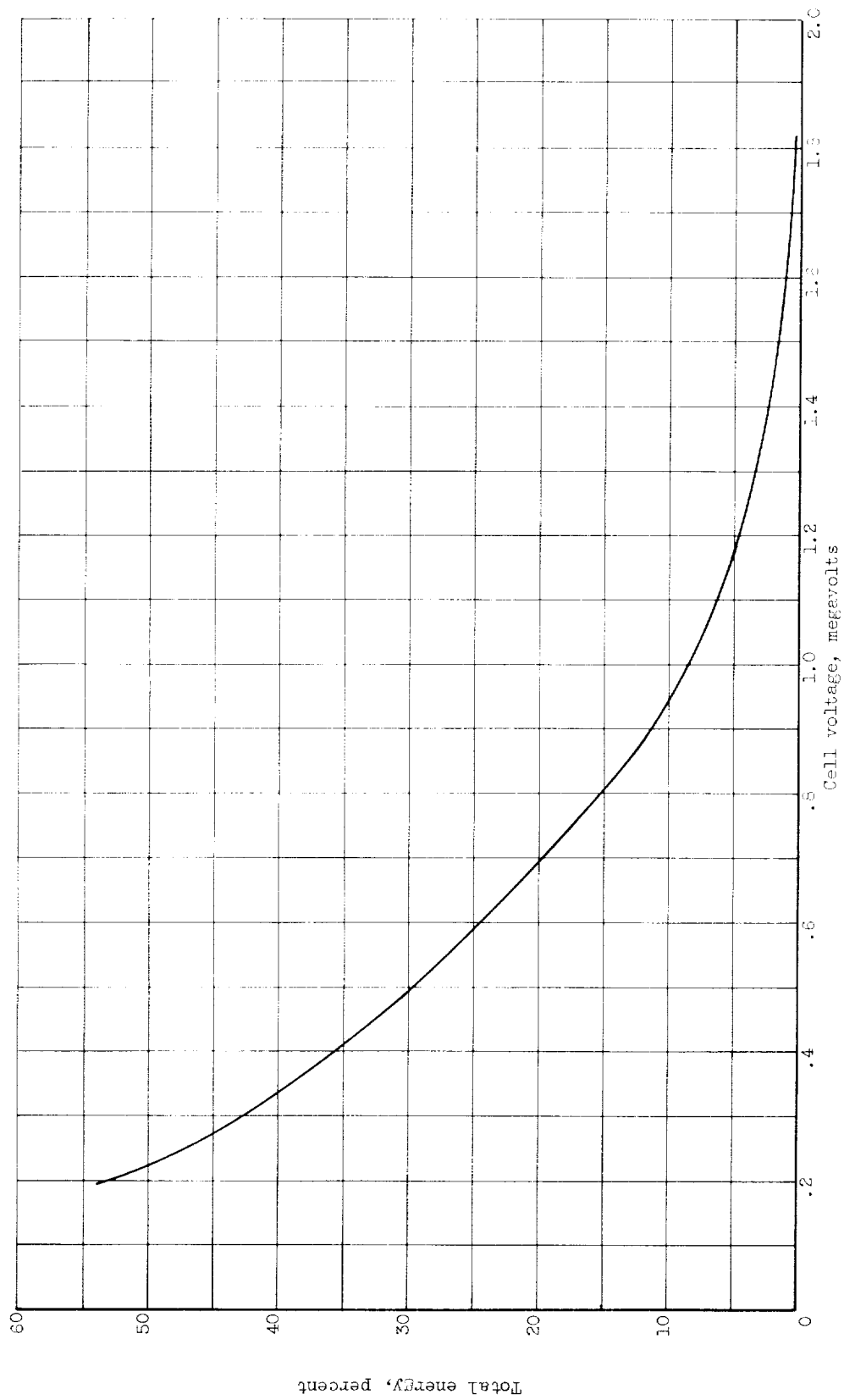
(b) Cylindrical Configuration.

Figure 2. - Concluded. Cell efficiency as a function of cell voltage for various radius ratios. Fuel-layer thickness, 35.0 milligrams per square centimeter; support-layer thickness, 25.9 milligrams per square centimeter.



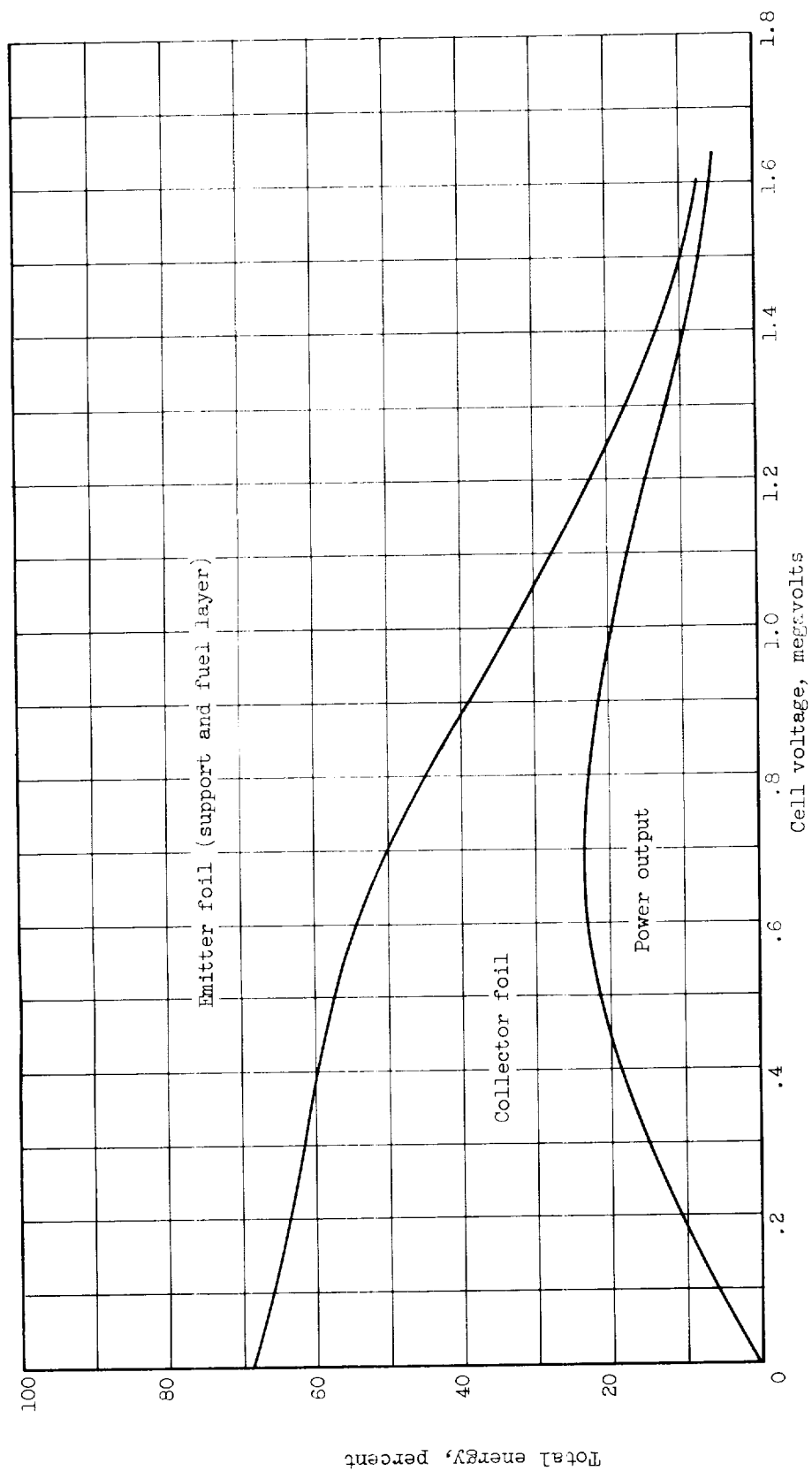
(a) Spherical configuration.

Figure 3. - Total energy reaching collector as a function of cell voltage. Fuel-layer thickness, 35.0 milligrams per square centimeter; support-layer thickness, 25.9 milligrams per square centimeter; radius ratio, 2.0.



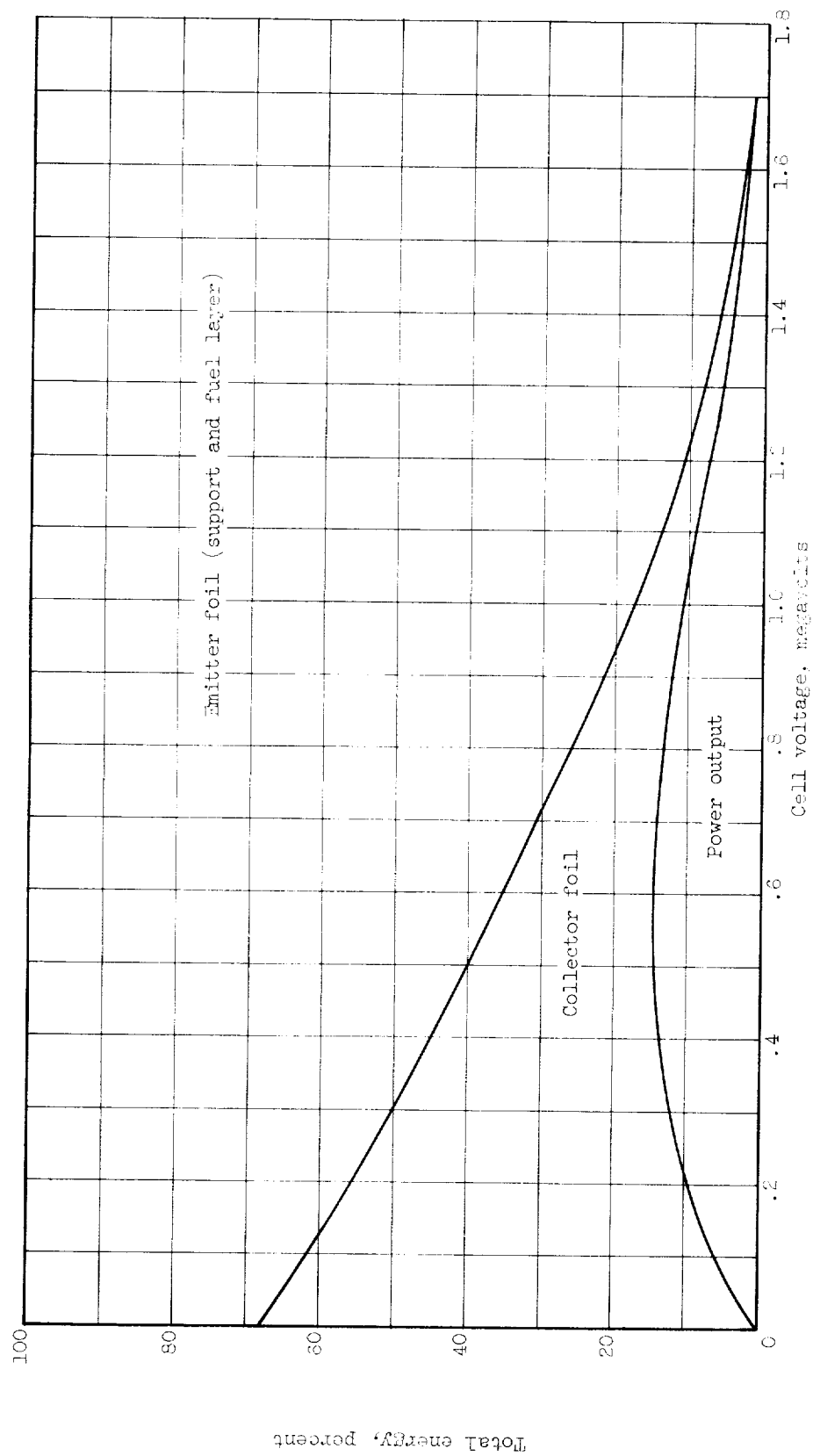
(b) Cylindrical configuration.

Figure 3. - Concluded. Total energy reaching collector as a function of cell voltage. Fuel-layer thickness, 35.0 milligrams per square centimeter; support-layer thickness, 25.9 milligrams per square centimeter; radius ratio, 2.0.



(a) Spherical configuration.

Figure 4. - Energy distribution in various cell components. Fuel-layer thickness, 70.0 milligrams per square centimeter; support-layer thickness, 25.9 milligrams per square centimeter; radius ratio, 2.0.



(b) Cylindrical configuration.

Figure 4. - Concluded. Energy distribution in various cell components. Fuel-layer thickness, 70.0 milligrams per square centimeter; support-layer thickness, 25.0 milligrams per square centimeter; radius ratio, 2.0.

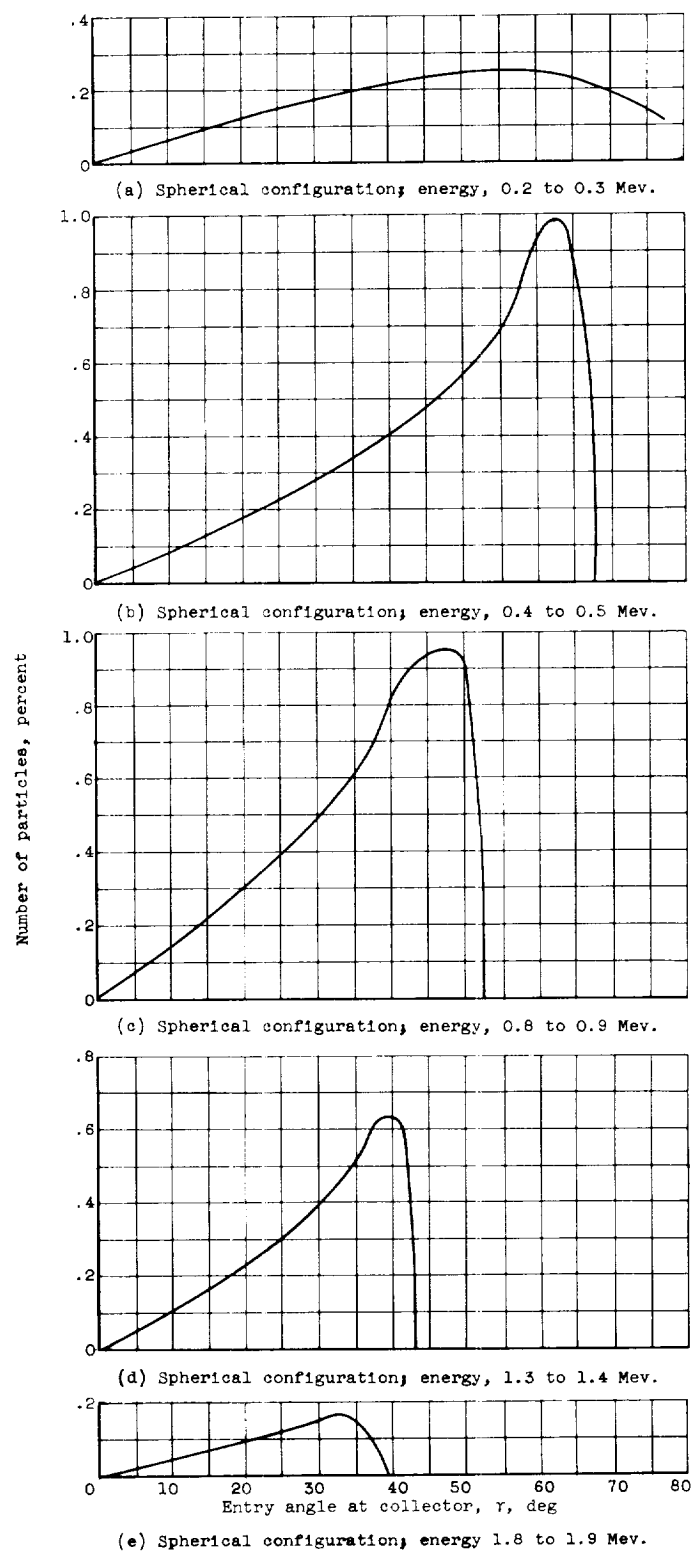


Figure 5. - Particle distribution at collector. Fuel-layer thickness, 35.0 milligrams per square centimeter; support-layer thickness, 25.9 milligrams per square centimeter; radius ratio, 2.0; cell voltage, 0.6 megavolts.

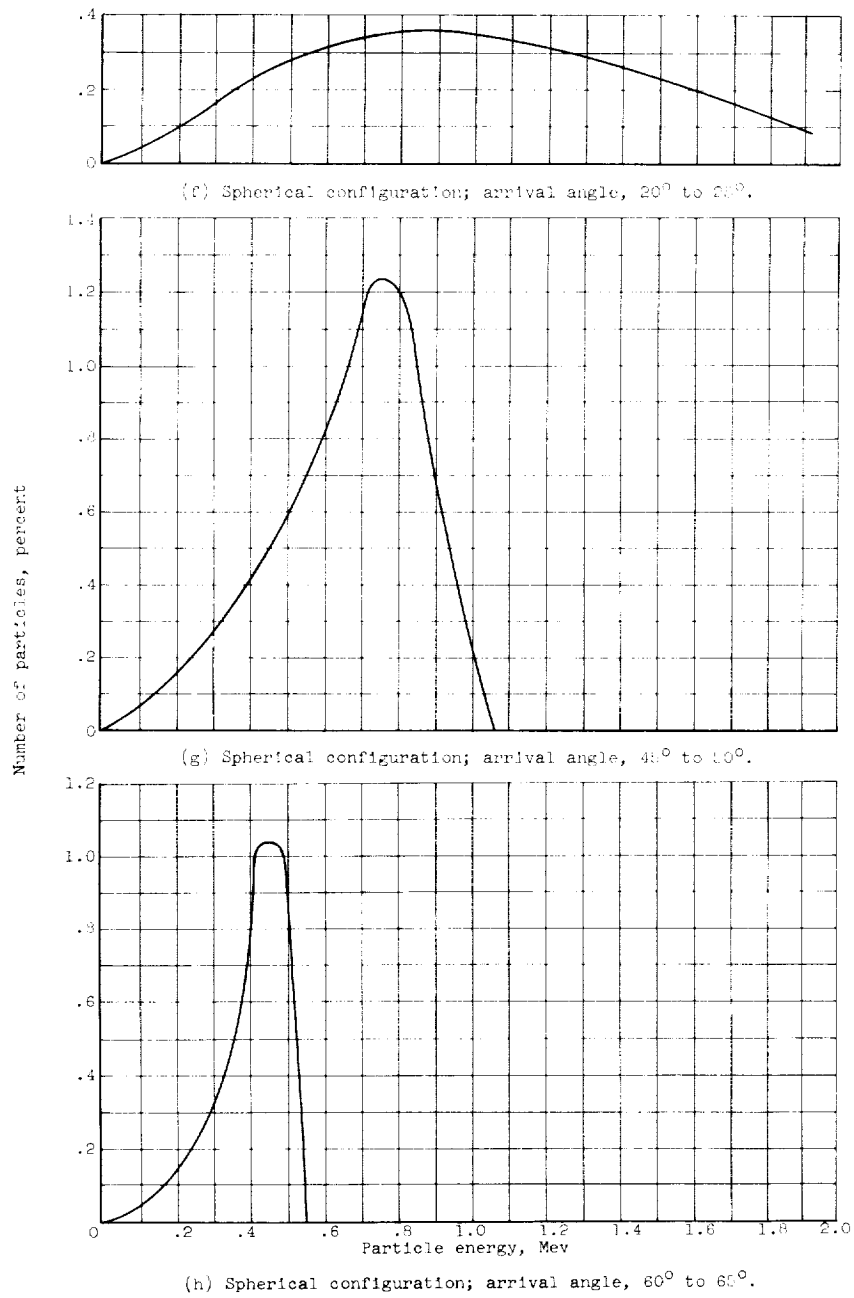


Figure 5. - Continued. Particle distribution at collector. Fuel-layer thickness, 35.0 milligrams per square centimeter; support-layer thickness, 25.2 milligrams per square centimeter; radius ratio, 2.0; cell voltage, 0.6 megavolts.

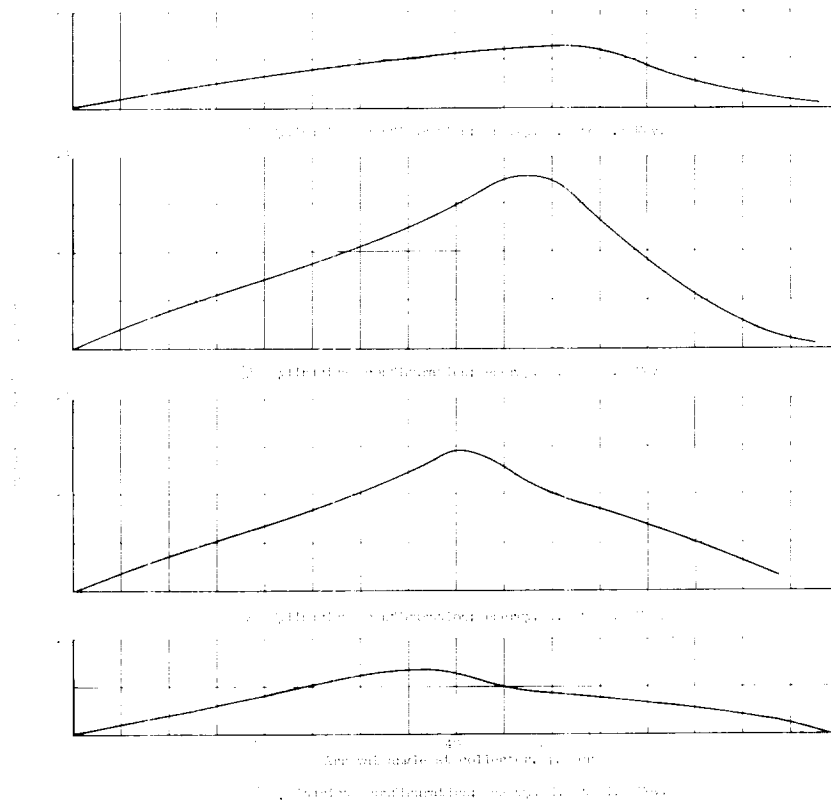
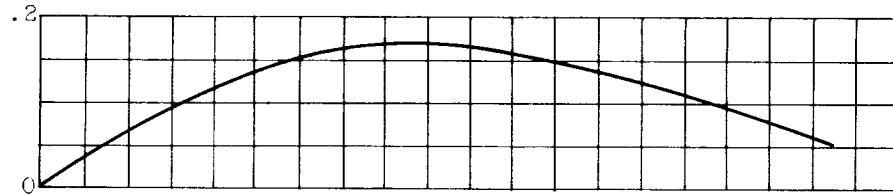
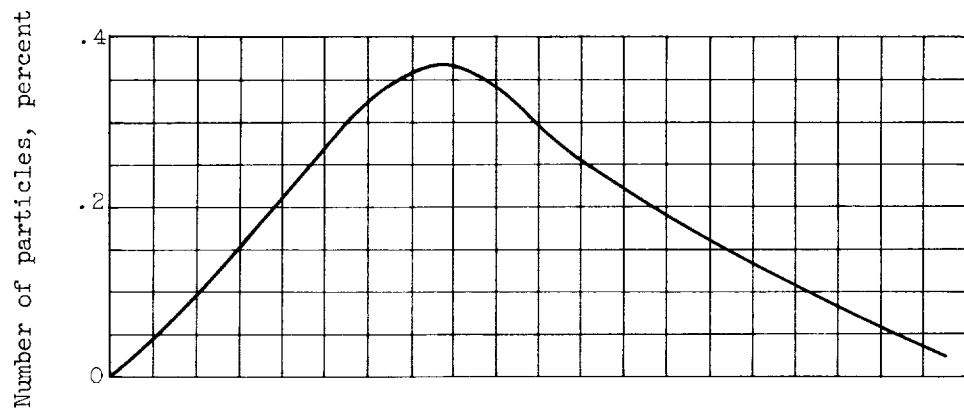


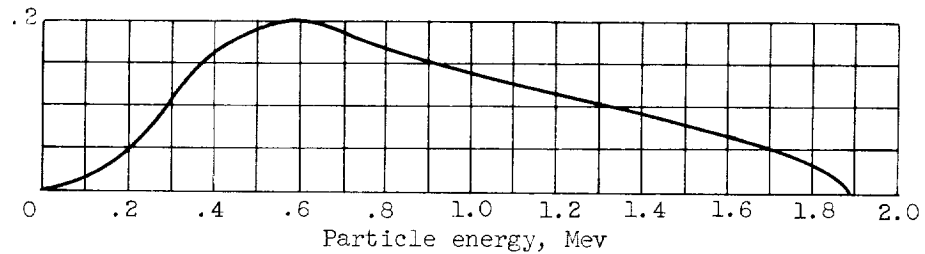
Figure 1. Particle distribution profiles for different collector types. (a) Flat-plate collector, (b) parallel-plate collector, (c) cylindrical collector, and (d) spherical collector. The y-axis is particle distribution and the x-axis is distance from collector, cm.



(m) Cylindrical configuration; arrival angle 20° to 25° .



(n) Cylindrical configuration; arrival angle, 45° to 50° .



(o) Cylindrical configuration; arrival angle, 60° to 65° .

Figure 5. - Concluded. Particle distribution at collector.
 Fuel-layer thickness, 35.0 milligrams per square centimeter;
 support-layer thickness, 25.9 milligrams per square centimeter,
 radius ratio, 2.0; cell voltage, 0.6 megavolts.

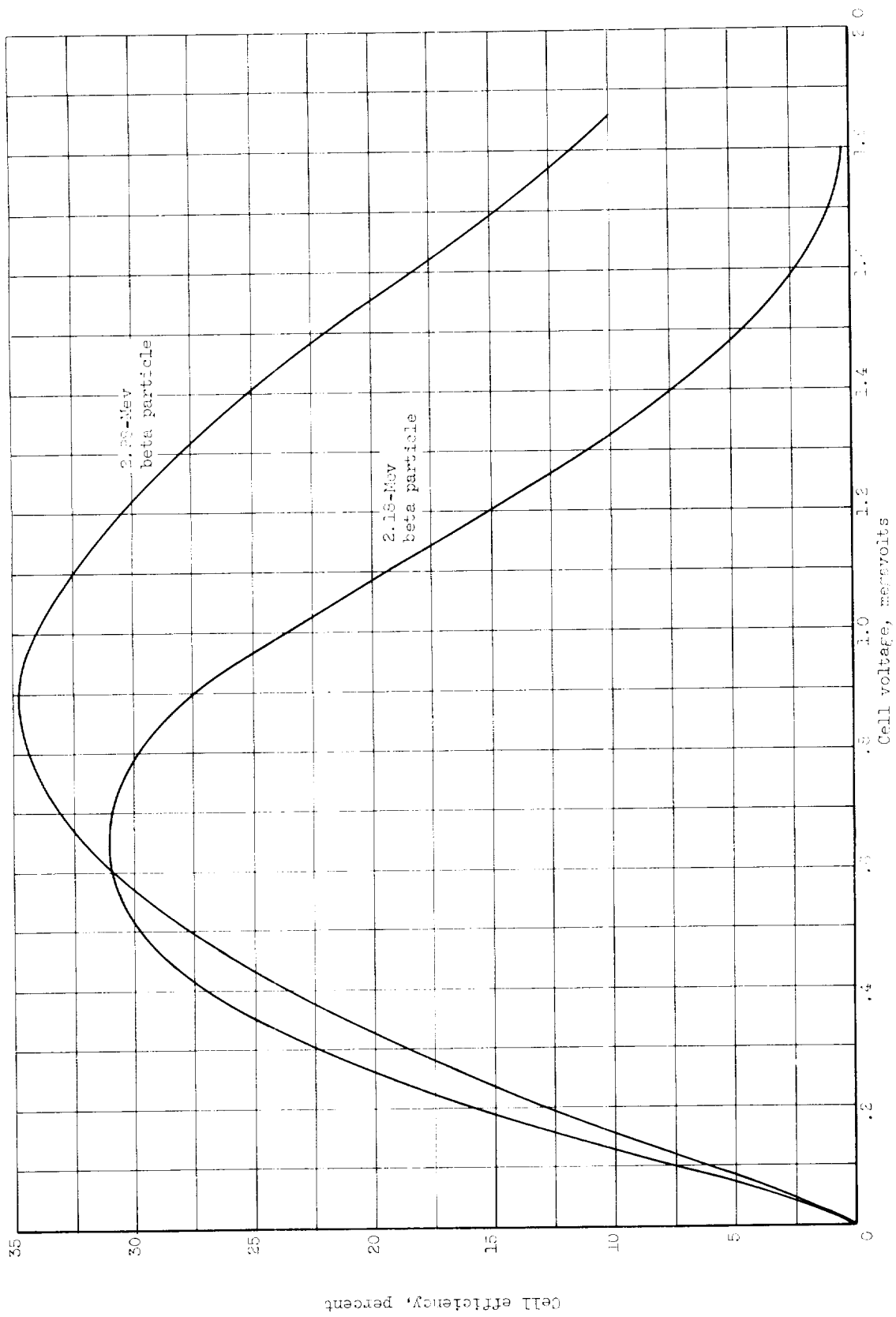


Figure 6. - Comparison of different beta-particle sources in efficiency calculation for spherical configuration. Fuel-layer thickness, 25.0 milligrams per square centimeter; support-layer thickness, 15.6 milligrams per square centimeter. Ratio ratio, 4.0.

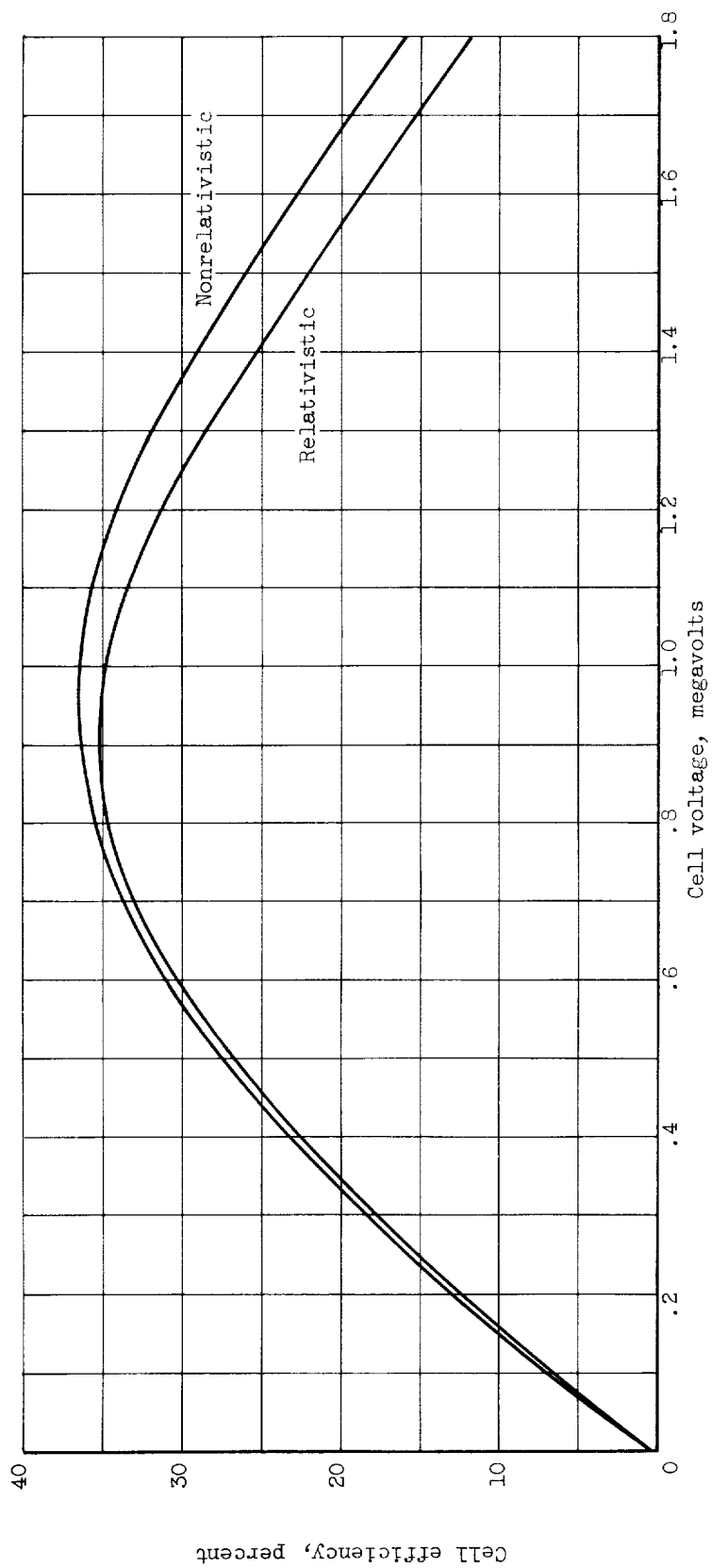


Figure 7. - Comparison of relativistic against nonrelativistic formulations in cell efficiency calculation for spherical configuration. Fuel-layer thickness, 35.0 milligrams per square centimeter; support-layer thickness, 12.9 milligrams per square centimeter; radius ratio, 4.0.

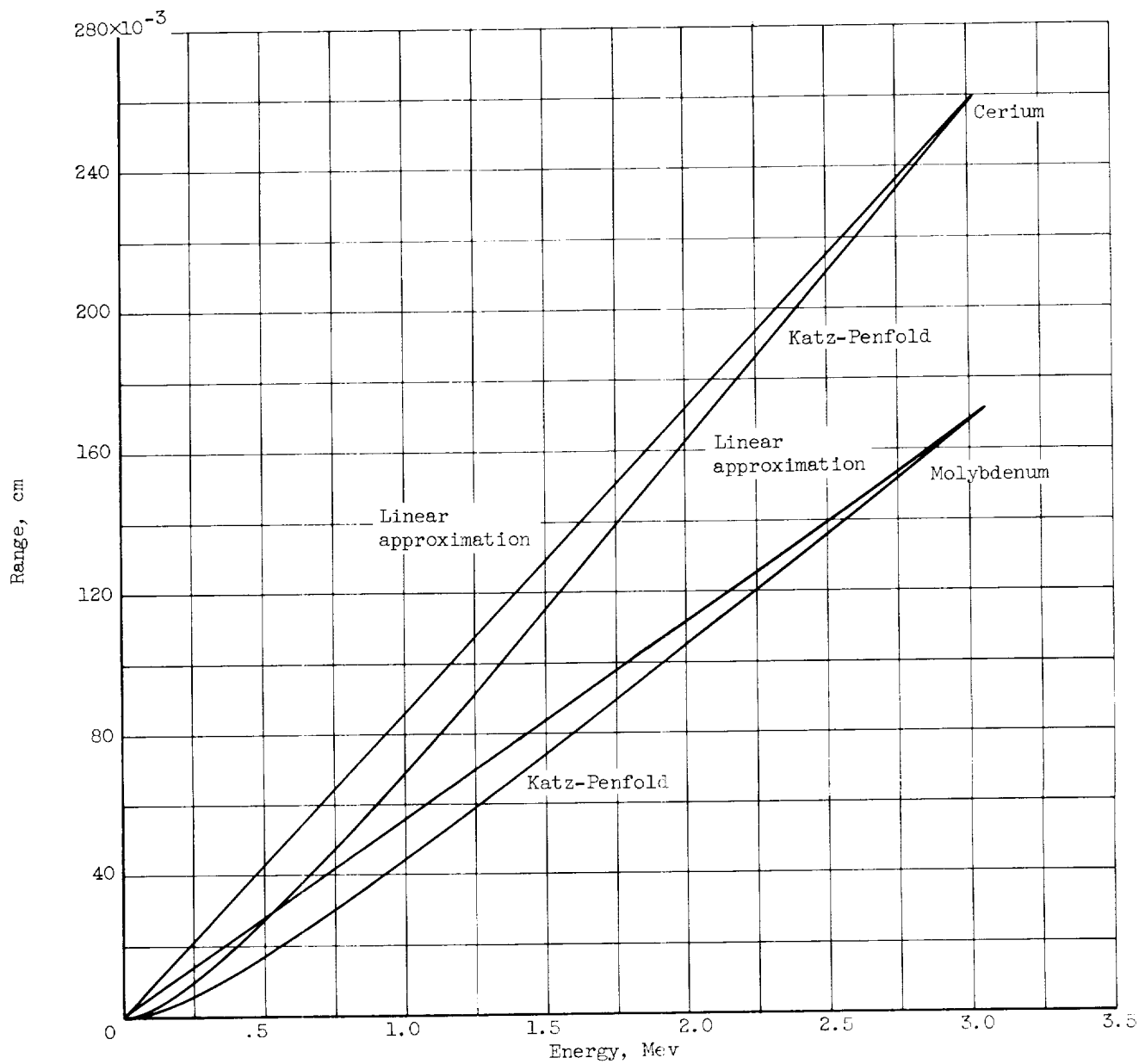


Figure 8. - Range-energy relations for beta particles in cerium and molybdenum.

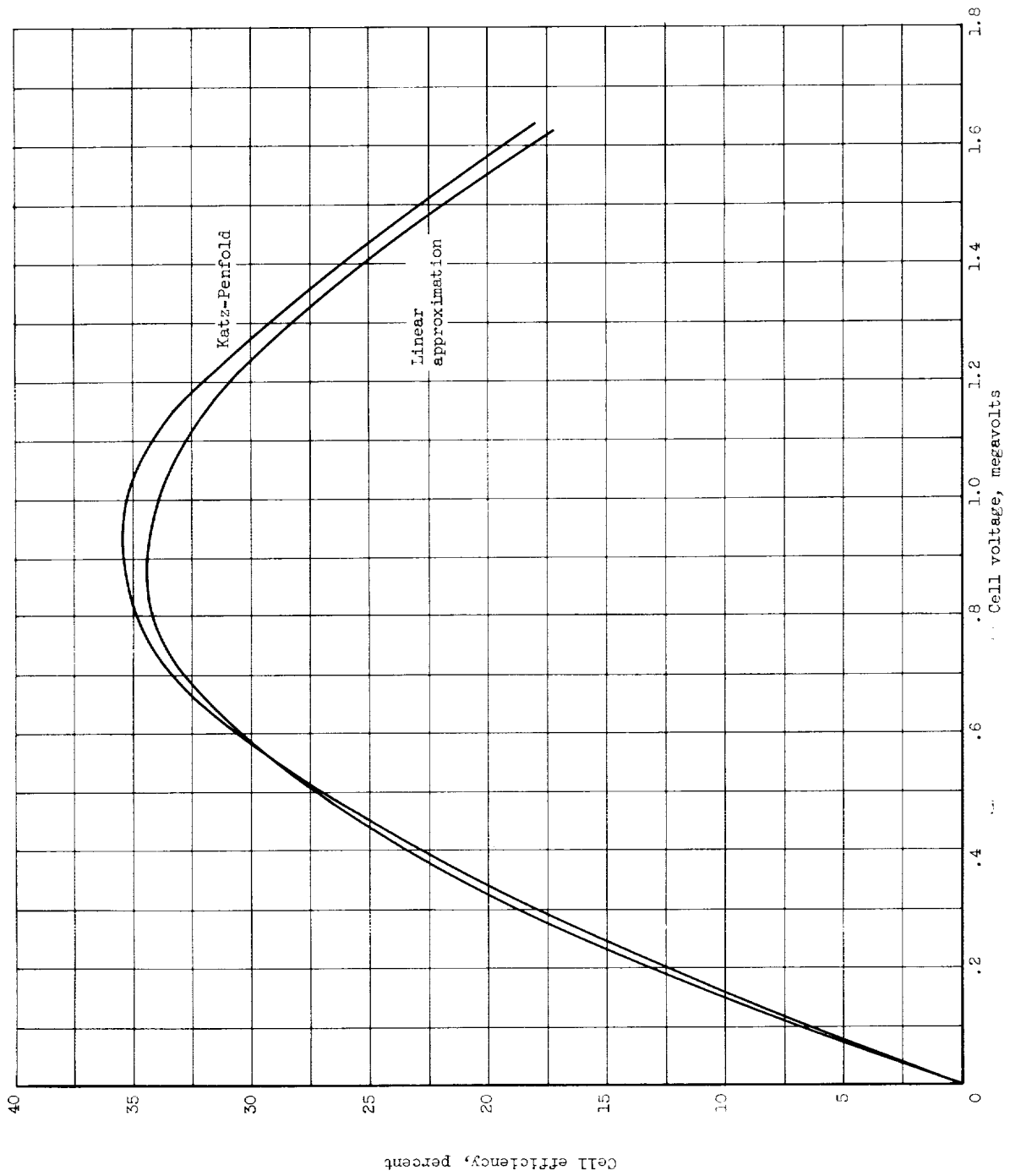


Figure 9. - Comparison of different range-energy relations in efficiency calculations for spherical configuration. Fuel-layer thickness, 35.0 milligrams per square centimeter; support-layer thickness, 12.9 milligrams per square centimeter; radius ratio, 4.0.